electronics

MDPI

Article

Underwater Antenna Technologies with Emphasis on Submarine and Autonomous Underwater Vehicles (AUVs)

Dimitrios G. Arnaoutoglou [1,2], Tzichat M. Empliouk [1], Dimitrios-Naoum Papamoschou [1], Yiannis Kyriacou [2], Andreas Papanastasiou [2], Theodoros N. F. Kaifas [1] and George A. Kyriacou [1,*]

[1] Department of Electrical and Computer Engineering, Democritus University of Thrace, 67100 Xanthi, Greece; darnaout@ee.duth.gr (D.G.A.); templiou@ee.duth.gr (T.M.E.); dimipapa111@ee.duth.gr (D.-N.P.); tkaifas@ee.duth.gr (T.N.F.K.)

[2] Ecliptic Defence and Space Ltd., 2251 Nicosia, Cyprus; ioannis.kyriakou@ecliptic-ds.com (Y.K.); andreas.papanastasiou@ecliptic-ds.com (A.P.)

* Correspondence: gkyriac@ee.duth.gr

Abstract

Following the persistent evolution of terrestrial 5G wireless systems, a new field of underwater communication has emerged for various related applications like environmental monitoring, underwater mining, and marine research. However, establishing reliable high-speed underwater networks remains notoriously difficult due to the severe RF attenuation in conductive seawater, which strictly limits range coverage. In this article, we focus on a comprehensive review of different antenna types for future underwater communication and sensing systems, evaluating their performance and suitability for Autonomous Underwater Vehicles (AUVs). We critically examine and compare distinct antenna technologies, including Magnetic Induction (MI) coils, electrically short dipoles, wideband traveling wave antennas, printed planar antennas, and novel magnetoelectric (ME) resonators. Specifically, these antennas are compared in terms of physical footprint, operating frequency, bandwidth, and realized gain, revealing the trade-offs between miniaturization and radiation efficiency. Our analysis aims to identify the benefits and weaknesses of the different antenna types while emphasizing the necessity of innovative antenna designs to overcome the fundamental propagation limits of the underwater channel.

Keywords: underwater antennas; underwater communication; Autonomous Underwater Vehicles (AUV)

1. Introduction

In recent years, there has been a growing focus on the development of underwater electromagnetic (EM) systems that stems from the need to support wireless communications in a variety of practical systems and applications. Those include Underwater Sensor Networks (UWSNs), communication tools for scuba divers, Autonomous Underwater Vehicles (AUVs), and Remotely Operated Vehicles (ROVs) with the list being far from complete. These are amplified by the fact that the sensing capability of EM waves offers critical superiority against acoustical methods due to their immunity against waves, Doppler shift, and multi-path effect. Some possible applications include Object and Mine Detection, Seabed Mapping, Non-Acoustic Subsurface Inspection, Archaeology Infrastructure Monitoring, and Environmental Sensing. These applications play a critical role in marine exploration, oil and gas pipeline monitoring, environmental data collection, and coastal surveillance. For instance, environmental inspection in sea becomes crucial to enhance a great number

Academic Editor: Djuradj Budimir

Received: 6 December 2025
Revised: 25 December 2025
Accepted: 29 December 2025
Published: 2 January 2026

of activities like tourism, fishing and aquaculture. To achieve this, collection of periodic submarine data is essential from fixed probes (installed at different sites) or even from AUVs capable of relocating in real-time for measurements. In addition, reliable underwater communication and sensing systems are crucial in the challenging marine environment for military applications where collaboration is needed between submarines, AUVs, and divers. Furthermore, advanced underwater antennas can provide strategic advantages by ensuring secure and low-detectability communication channels in contested waters.

WSNs have increasingly become a prominent area of research due to their affordability and significant value in the military and commercial sectors [1]. UWSNs typically include stationary sensor nodes (such as cabled seafloor sensors, moored devices, and surface buoys) and mobile sensor nodes (such as autonomous/remote/unmanned underwater vehicles) [2]. Unlike terrestrial environments, the underwater environment presents unique challenges due to its conductive nature. As a result, achieving high-speed and reliable data transmission in such conditions is particularly difficult [3]. To enhance network coverage and maintain reliable operation, it is crucial to ensure efficient and robust data transmission between nodes. Thus, the communication network in such applications, especially when collaborative missions are taken place, must present high-data rate for data exchange between the communication nodes (including AUVs, fixed-probes and access point). For tasks involving short distances, particularly when high-speed transmission is needed—such as during vehicle coordination or data retrieval at docking stations—establishing Mbps-level data rates becomes vital for enabling complex operations such as AUV swarming [4]. Although wired solutions exist, they present limitations such as high installation costs, restricted mobility, and susceptibility to physical damage—especially over long distances or during extended deployments. The wireless communication approach allows for the establishment of a highly versatile network equipped with the ability to support movable AUVs exploring or monitoring different areas without the need of carrying a long cable which will degrade their agility and range of operation.

Historically, acoustic and ultrasonic technologies have served as the cornerstone of underwater communication due to their ability to transmit over long distances, often spanning several kilometers [5]. Acoustic waves propagate longitudinally along the direction of the propagation channel through alternating compression and expansion. In general, acoustic systems offer high efficiency and compact sizes at a low cost. However, they suffer from significant drawbacks: high latency, strong susceptibility to noise interference, and generally low data rates. In addition, acoustic signals are prone to multipath fading and Doppler shifts. In addition, they can affect marine ecosystems by causing harm or altering the behavior of marine mammals [5]. For example, human-generated noise in the ocean can disrupt the detection of natural acoustic signals, effectively masking the sounds of marine animals. This interference can alter individual and group behavior, affect metabolic processes, and hinder reproduction and population growth. Consequently, these disruptions can undermine the health and ecological integrity of marine ecosystems [6].

In response to these limitations, researchers have explored alternative data transmission methods [5], the most widespread are optical and EM systems. Although neither of these alternatives can match the long-distance capabilities of acoustic waves—owing to the strong absorption of signals in water—they offer significant advantages for short-range links. In optical systems, laser and other light sources are utilized to connect two points. Optical communication supports high data rates (up to Gbps) and low latency but it requires precise alignment and can be disrupted by particles and marine bio-fouling. Especially in shallow water, the increased presence of plankton makes the establishment of a link a challenging task, prohibiting the data transmission between the air-sea interface [7]. One significant challenge is the dispersive underwater particles, which influences both the po-

larization and transmission characteristics of light waves [5]. Thus, optical communication systems are ideally suited for applications requiring the rapid exchange of large volumes of information, such as underwater video and image transmission [8].

EM waves, particularly in the high-frequency (HF) band, experience significant attenuation, but are less affected by water turbidity or alignment constraints. These facts make them suitable for short-range scenarios such as AUV-to-AUV link which can be critical for decentralized mesh-type communication networks as depicted in Figure 1. Early work in underwater EM communications began in the 1960s but remained largely theoretical due to technical constraints, primarily the severe attenuation of HF signals in water [9]. A recent study indicates that RF communication in the HF band can achieve reliable data rates of up to 6.8 Mbps in short ranges, without demanding precise alignment or clear water conditions [10]. This makes EM-based systems promising for specific underwater applications where short-range, high-speed, and robust communication is required.

The exceptionally high propagation speed of EM waves (compared to acoustic waves) greatly reduces communication delays in underwater environments, simplifying the design and implementation of networking protocols such as medium access control (MAC), routing, and sensing services (e.g., localization). At the physical layer, synchronization between devices becomes more straightforward and reliable due to the minimal delay and stable channel conditions. Whereas acoustic and optical methods rely on audible sound or visible light, magneto-inductive (MI) communication employs non-audible, non-visible waves, enabling secure operations suitable for both civilian and military purposes [11]. One practical use involves swarms of AUVs or ROVs operating in close formation to establish a communication relay chain, effectively creating a relay network [12]. In cluttered underwater environments—such as leaking submarine compartments, shipwrecks, or fully submerged buildings—bulky vehicles and conventional acoustic systems face severe limitations due to restricted spaces and severe multipath fading, which degrades channel quality. In these cases, compact, agile underwater robots equipped with small RF antennas can navigate tight, complex spaces more efficiently, providing reliable communication where other methods fail.

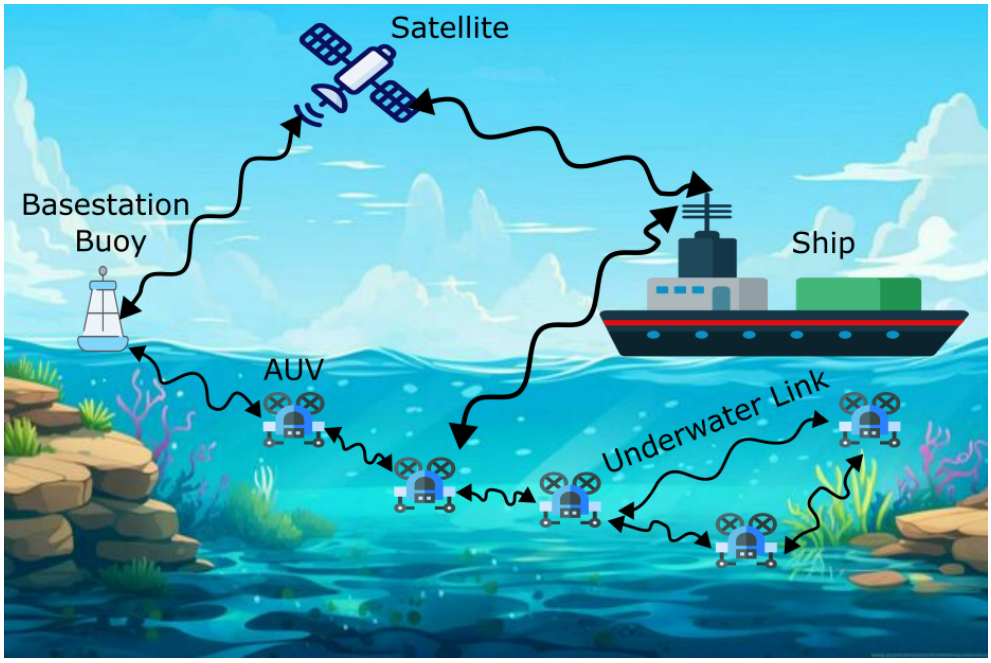

Figure 1. An example of a decentralized communication network consisting of AUVs.

The review article is organized as follows. Section 2.1 provides a brief review of RF propagation characteristics in water. In Addition, it presents an analysis of experimental studies demonstrating that lower attenuation losses can be achieved in seawater environments. In Section 2.2, the fundamental antenna design requirements for underwater applications are presented. In detail, design considerations for their integration into commercial AUVs and ROVs are discussed without degrading their operation. In Section 2.3, the operation and benefits of near-field coupling using MI loop antennas are elucidated. In Section 2.4, different shapes of dipole antennas are presented, highlighting their advantages and disadvantages when they are submerged in water-like environments. Following this, in Section 2.5, a novel design approach of directive antennas for point-to-point applications is presented, illustrated through the example of horn antennas arranged in circular arrays. In Section 2.6, miniaturized antennas based on the mechanical interaction of two different phases (piezoelectric and magnetostrictive) are analyzed, permitting operation in lower frequency ranges while maintaining a compact structure. Next, various configurations of planar patch antennas are presented that can be incorporated on the surface of underwater systems (Section 2.7). Finally, in Section 2.8, the benefits and drawbacks of each antenna type are summarized and analyzed, providing a comprehensive review for any designer seeking to pursue the development of underwater antennas.

2. Materials and Methods

2.1. Underwater Electromagnetic Propagation

Although EM waves experience significant attenuation and energy loss in water—particularly in seawater—compared to air. To compensate for these losses underwater RF communication systems operate at low frequency permitting a short-range underwater propagation. This makes EM-based systems a promising alternative in scenarios where traditional methods, such as acoustic or optical communication, are impractical or inefficient.

Currently, EM techniques are primarily employed to enable communication between military submarines and land-based control centers, playing a critical role in defense and national security. EM waves propagate effectively through air, water, and across their interface, and their minimal Doppler effect enhances reliability for submarine operations. In air propagation, the dominant attenuation factor is free-space loss, which results from the signal's energy dispersing as it radiates outward [13]. The biggest challenge of RF propagation in underwater applications is not the spatial spreading but the severe attenuation due to the seawater conductivity. For a simple example, the attenuation coefficient for an 1 MHz acoustic wave propagating in seawater is lower than 0.1 dB/m, while at the same frequency the EM waves display values above 33 dB/m. To minimize conduction losses, the operation of a compact RF system at low frequencies (below 1 GHz) was proposed in the literature [5,14].

Seawater presents a highly complex medium for RF propagation due to the various dissolved chemical constituents that influence signal's behavior. For the purposes of this study, the propagation region within seawater is assumed to be locally isotropic. As a partially conductive medium, seawater exhibits high permittivity (ϵ), which contributes significantly to the attenuation of the electric field component of an electromagnetic wave. Since seawater is non-magnetic, its magnetic permeability (μ) is taken to be equivalent to that of air. Regarding its permittivity, seawater presents the same dipolar nature like fresh or distilled water. These dipoles are due to the asymmetric bonds of oxygen-to-hydrogen resulting to intense interaction with electric fields. The presence of numerous dissolved salts in water, particularly sodium chloride (NaCl), results in high ionic concentration and, consequently, elevated conductivity. At low EM frequencies of a few MHz the seawater di-

electric constant is about $\epsilon_r = 90$ while its conductivity varies between 2–4 S/m depending on the concentration of NaCl.

The electrical conductivity of seawater can be separated into two components: the first (σ') arises from the ionic conduction currents generated by ions such as Na^+ and Cl^-, while the second (σ'') is associated with dielectric dipole losses, generating displacement currents. Instead of an equivalent conductivity (σ'') for the displacement current, this phenomenon can be accounted through the imaginary part of permittivity (ϵ''). This term represents the energy loss caused by the water dipole oscillations. Hence, it appears in both fresh, distilled, and seawater. Both of these current mechanisms interact with any applied EM radiation.

Assuming a harmonic plane wave of angular frequency ω_0 propagating inside a non-magnetic and homogeneous medium, the electric field (E) obeys the formula:

$$E = E_0 e^{j\omega t - \gamma z} \tag{1}$$

where E_0 is the amplitude of the signal at the origin of the reference coordinate system ($z = 0$) and $\gamma = j\beta + a$ is the complex propagation constant. The propagation constant consists of two terms: one responsible for the propagation (β) and the other for the attenuation losses (a). The β and a can be described with the following relation [15]:

$$\gamma = j\beta + a = \sqrt{j\omega\mu(\sigma + \omega\epsilon'' + j\omega\epsilon')} \tag{2}$$

where σ is the conductivity of the medium (S/m), $\epsilon = j\epsilon'' + \epsilon'$ is the complex permittivity including the energy store (ϵ') and dielectric loss (ϵ'') term. Calculated by Equation (2), the attenuation coefficient of an EM signal inside different types of water (distilled, fresh and sea) is displayed in Figure 2 for the frequency range between 10 kHz and 100 MHz. The EM characteristics of each medium are presented in Table 1, where ϵ'' can be calculated using Debye's equation [15]:

$$\epsilon'' = (\epsilon' - \epsilon'_\infty)\frac{\omega\tau}{1 + \omega^2\tau^2} \tag{3}$$

As can be observed, the loss is enormous for the case of seawater with a conductivity $\sigma_{sea} = 4$ S/m for salinity 3% and temperature at 25 °C. In contrast to the case of tap and distilled water ($\sigma_{tap} = 0.0015$ S/m and $\sigma_{dist} = 0.0002$ S/m), where the introduced losses can practically permit the propagation of EM waves. Based on the results shown in Figure 2, establishing an EM link beyond 10 m appears infeasible. Nevertheless, there are results in the open literature that suggest otherwise. Indeed measurements reported in [15–18], conducted offshore near Liverpool's port, reveal a peculiar behavior: the received signal experiences severe attenuation at short distances, whereas at longer ranges the attenuation deviates from the prediction of Equation (2). This behavior was observed in the range of a few MHz [18]. The authors of [18] tried to explain this behavior with the introduction of dielectric dipoles of sea water waves in water. In this case, the wave propagates inside a virtually formed waveguide attenuating lower than the conventional EM waves [18]. It is impressive that a similar "self guiding" phenomenon is already well known in magnetized plasma media supporting very low loss wave propagation, [19]. This is also observed in ionospheric EM wave propagation (Whispering-gallery wave) [20] supporting low loss communication between the earth's poles. Since the ionosphere consists of ions, a similar propagation mechanism could be anticipated in seawater.

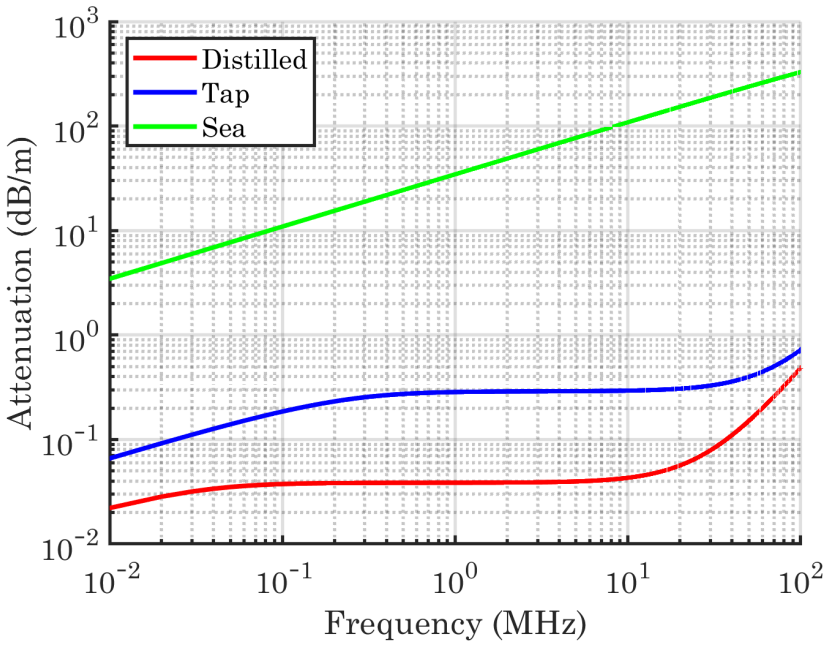

Figure 2. Attenuation coefficient of (**a**) distilled-, (**b**) tap- and (**c**) seawater at range 10 kHz to 100 MHz. The used ϵ_r and σ are depicted in Table 1.

The challenge in this approach is to effectively stimulate dipole waves using a small antenna. In [15], a potential design was proposed deploying a loop-shaped antenna. Despite these efforts, the dipole wave mechanism was abandoned by the researchers. Nevertheless, a similar trend of low loss propagation was identified in [21–24], where the authors tried to justify these results by the generation of surface waves near the sea-air interface and/or sea-seafloor. In [24] a channel modeling based on the Goos-Hänchen shift indicates that the main path of the propagating wave for medium and long distances in seawater is the seawater–air path and seawater–seafloor path verifying the experimental results of authors' previous work [25]. These results show that the measurements on the Liverpool dock [16,17] may be the result of surface waves due to the low depth of sea at which the measurements were taken. A summary of the multipath propagation of the RF wave inside shallow water is depicted in Figure 3 highlighting all potential propagation paths.

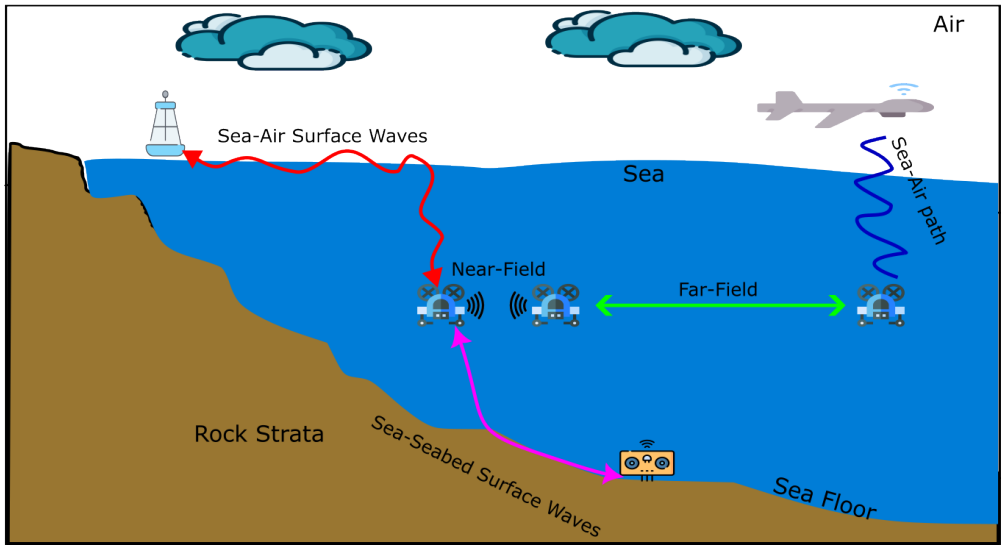

Figure 3. Different RF propagation paths for Underwater Sensor Networks, AUVs, Buoy and UAVs.

To numerically validate the above assumption, an EM simulation was conducted in CST Studio to model the interaction between two underwater antennas in shallow water. We investigated three different operating depths, with air–water interface and the seabed explicitly included in the simulation domain. The water depth was set to 5 m, and the antennas, modeled as simple insulated dipoles, were placed at equal depths with varying separation distances. The received signal's strength at 1 MHz is presented in Figure 4. The simulated results reveal a steep attenuation in the near-field region, characterized by a loss of approximately 40 dB/m within the first 4 m. Beyond this range, when antennas are positioned closer to the water surface or the seabed, the signal attenuates smoother, with an attenuation factor of approximately 2.7 dB/m, consistent with theoretical predictions reported in [22]. In contrast, when the antennas are located midway between the two boundaries, only the steep attenuation mechanism (40 dB/m) is observed, suggesting that proximity to the surface or seabed facilitates the excitation of surface-wave modes with lower attenuation. It is important to note that the stabilization of the received signal observed at approximately 10 m is an artifact of the numerical solver, resulting from the finite resolution of CST Studio in handling the system's large dynamic range. Furthermore, the antennas considered in this study were not optimized for underwater operation, which explains the very low received power levels (below −200 dBw). Nevertheless, with a suitable antenna and the integration of amplification techniques, reliable underwater communication over distances exceeding 50 m remains achievable. Interestingly, the peculiar 1/R dependency reported in [16] was not reproduced in these simulations, implying that the mechanism of dipole-wave propagation [18] may indeed play a significant role in underwater EM transmission. However, for this latter option, there are not yet enough scientific findings proving the existence of a dipole-wave propagation or a virtual waveguide in which the signal can effectively propagate.

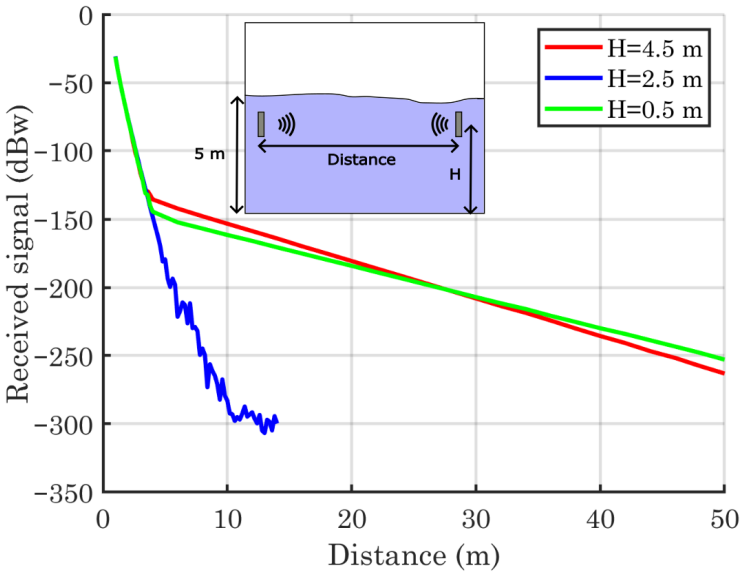

Figure 4. Received signal for a EM wave propagating in seawater for a distance of 100 m at T = 25 °C.

Table 1. EM properties of different water media at 25 °C [15,26].

Medium	σ (S/m)	ϵ'	ϵ'_∞	τ (ps)
Distilled Water	0.0002	72	3	9.6
Tap Water	0.0015	72	3	9.3
Seawater	4	72	3	8.2

2.2. Design Requirements for Optimal Antennas Enabling Underwater Communication and Sensing

In contrast with terrestrial and non-terrestrial communication and sensing systems, there are not yet explicitly defined standards or limits for power and frequency. For power, due to the lossy nature of the seawater and the lack of human beings in close vicinity there have not yet been established limits for the transmitters. For that reason, the most works either adopt the power transmitted by a mobile or terrestrial transmitter depending on the implemented protocol LoRA, Wifi, or use a high-power module in order to ensure the successful reception of the signal at the receiving node. Similar reasoning holds true for the frequency allocation for underwater application; due to the high loss, it is impossible to interfere with the allocated bands of mobile and satellite communications, especially if the applied area is in the middle of the sea. The ITU have allocated some Very Low Frequency (VLF) bands for submarine communication (around 3–30 kHz) but these allocations are established for radio services and not specifically for underwater communication or sensing systems [27]. In addition, the lack of regulatory limits is attributed to the limited existence of commercial underwater RF communication systems, leaving the field undirected. However, if more commercial products and services begin to emerge, creating congested environments of WSN, it is highly likely that regulations will be enforced from international and national organizations. For now, RF underwater communication is an undiscovered and unexploited area of research effort.

Beyond the physical optimization of individual radiating elements, the design of underwater antennas must be intrinsically linked to the broader system-level requirements of UWSNs and the Internet of Underwater Things (IoUT) [28,29]. Recent system-level studies emphasize that the severe bandwidth limitations and high attenuation of the underwater channel necessitate a cross-layer design approach, where the physical layer attributes, which are constrained higher-layer by performance metrics such as network throughput, latency, and routing reliability. Consequently, the antenna cannot be treated as an isolated component; its integration must account for the dynamic link quality and energy constraints inherent to battery-operated underwater nodes [30].

This interdependence is particularly critical in the deployment of multi-AUV networks and swarm robotics. Practical scenarios include cooperative sensing, formation control, and survey missions, all of which require robust and resilient inter-vehicle communication that becomes especially important due to the continuous motion of ROVs and AUVs [30]. In such dynamic network topologies, antenna spatial coverage becomes a decisive factor for overall network stability. For example, while high-gain directional antennas are well suited for static, point-to-point data offloading to a surface gateway, they often fail to maintain the continuous connectivity required for mobile swarms because of frequent misalignment and beamforming errors. In contrast, recent research on AUV swarms advocates the use of compact, omnidirectional radiators to mitigate the “hidden terminal” problem and ensure reliable telemetry exchange regardless of vehicle orientation [31].

To ensure connectivity among various underwater or surface systems (AUVs, Buoys, Ships, ROVs, and Satellites) for sea exploration, the development of novel antennas is critical. In this study, we are going to limit the scope around the underwater communication channel without considering the air link between the different systems (e.g., satellite with Buoys), because it can be studied as a general antenna system. As mentioned in the Section 1, nowadays underwater communication is dictated by acoustic systems capable of transmitting signal in long ranges (km), but they are hampered by low data rates and multipath fading. RF communication offers an alternative solution for short-range applications, enabling higher data rates and providing robust, reliable connectivity, as discussed in [14]. The most important element of such communication systems is the radiating element,

which will determine the coverage area of the system through the radiation pattern and efficiency. If we break down the process of designing an antenna—and, by extension, the rest of the communication system—the four main considerations are as follows:

- Frequency of operation,
- Omnidirectional or directive radiation patterns,
- Size and shape,
- Near or Far field coupling of antennas.

Higher frequencies enable wider bandwidth and, thus, higher data rates. At the same time, they limit the operating range/service coverage because the seawater attenuation coefficient increases with frequency, as displayed in Figure 2. Omnidirectional and isotropic radiation patterns ensure an unbiased angular communication probability around the node. However, in such cases, the antenna gain is minimized, decreasing the covered range of the antenna, so an appropriate analysis must be performed.

The size of the antenna is critical for small AUVs and ROVs used for mining and ocean exploration, especially if they operate as swarms. The footprint is directly related to its operating frequency and gain. Consequently, lower frequencies require bulkier antennas, which may be impractical for certain applications, thereby reducing efficiency when size constraints are imposed. An important consideration for antenna integration in AUVs and ROVs is the antenna's geometric design, as it significantly influences hydrodynamic efficiency and overall performance. For example, elongated antennas are difficult to mount because they protrude from the streamlined body, thereby increasing drag and degrading maneuverability. In the case of more complex antenna configurations, unlike the dipole antenna—which inherently requires no structural modification- and the loop antenna, whose geometry cannot be altered to satisfy the specified dimensional constraint, redesign is often necessary to ensure conformity with the external profile of the AUV.

Figure 5 illustrates four representative commercial AUVs/ROVs, where antenna locations are indicated by dashed circles. In these examples, integrated antennas are designed to support both submerged and surface-level communication. To minimize hydrodynamic penalties, antennas are embedded within protective housings or shaped like fins, ensuring that communication capability is achieved without compromising the underwater velocity and efficiency. One of the key challenges lies in designing innovative antenna systems and determining their optimal placement on the vehicle surface to ensure reliable communication without compromising its hydrodynamic performance or underwater maneuverability.

Finally, an important factor when designing an underwater system is the mechanism of coupling between the antennas. Near-field coupling can be achieved when the antennas ranging a distance around one wavelength (λ) where the communication is established with the reactive non-propagating electric or magnetic field around the antenna. Examples of such links include Near Field Contact (NFC) payments [32], wireless charging [33], and medical imaging and/or hyperthermia [34,35]. The benefits of near-field communication incorporate higher efficiency and low power demands for uninterrupted link. On the other hand, longer wavelengths (lower frequencies) are needed to support longer ranges in contrast with far-field link, where the link is only limited from free space loss and attenuation due to conductive sea water. This does not mean that the near-field coupling does not display attenuation losses, but because it relies at the near-field contact and the antenna is designed based on that, increasing the distance between the antenna introduces higher propagation losses compared to an antenna developed to operate in far-field. This can be attributed to the fact that near-field antennas are electrically short and have a low radiation efficiency. The communication range in underwater near-field systems is limited to within one wavelength; any multipath effect between the transmitter and receiver results

in minimal phase shifts. As a result, the coherence bandwidth greatly exceeds the system bandwidth, making channel distortion and fading practically negligible.

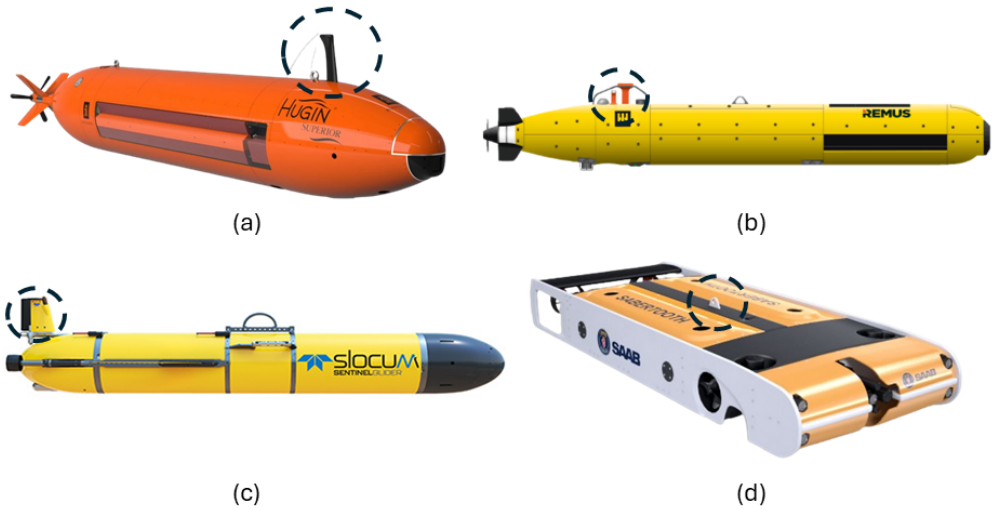

Figure 5. Different types of commercial type of UAVs/ROVs: (**a**) Kongsberg HUGIN [36], (**b**) REMUS 600 [37], (**c**) Teledyne Webb Research Slocum Glider [38] and (**d**) Saab Sabertooth [39]. With dashed lines are highlighted the position of EM antennas.

In the next sections, different antenna categories will be presented grouped on the aforementioned characteristics. Specifically, MI loop, dipole, directive antennas, magneto-electric, patch antennas will be analyzed. The metrics will be analyzed are: size, frequency, bandwidth, directivity and radiation efficiency. These metrics will be in a form of a table at the end of every subsection and then in the discussion Section 2.8 the overall comparison between the categories of the antennas will be described.

2.3. Magneto-Inductive Coupling Close Proximity Using Loop Antennas

In MI communication, data are transmitted through a time-varying magnetic field. This field is generated by a modulated sinusoidal current flowing through an MI coil antenna at the transmitter. The receiving coil antenna receives the produced magnetic near-field, which is then demodulated to recover the information. Considering the above principle of operation, the most popular antenna choice is magnetic dipole or current loops [40]. The range of MI for efficient operation is limited to one wavelength (λ) in the water medium.

MI communication systems prolong negligible signal propagation delay, predictable and constant channel behavior, sufficiently long communication range with high bandwidth, as well as silent and stealth underwater operations [31]. Because a coil antenna has much lower radiation resistance than an electric dipole, it radiates only a small fraction of energy into the far field. As a result, MI-based underwater communications are largely immune to multipath fading, a common issue in acoustic systems [31]. Furthermore, the fast propagation speed of MI waves minimizes frequency shifts caused by Doppler effects, making channel performance—in terms of data rate and packet loss—stable and predictable over a given range. Unlike optical systems, MI communications are unaffected by light scattering and water turbidity, ensuring consistent range and signal quality. Additionally, while acoustic and optical systems must contend with noise from sound and ambient light, MI channels experience relatively low electromagnetic noise underwater, as high-frequency interference is naturally attenuated by seawater.

The MI communication system consists of multi-loop coil antennas as shown in Figure 6 where the critical parameters are the number of turns (N), the diameter of loops

(D) and the angle between the receiver and the transmitter (θ). The coil's radius determine the frequency of operation and the number of loops the efficiency of the system. A trade-off is based on the specifications of the AUVs or ROVs in which the antenna will be placed. In MI communication, the term radiation pattern cannot be defined because the link is related to near-field, but some researchers included it in their study [41,42]. For underwater applications, MI dominates compared to capacitive coupling which is characterized by higher losses because of the strong generated electric field. Seawater exhibits finite electrical conductivity, which significantly attenuates the electric field. However, its magnetic permeability—and associated magnetic losses—remain nearly identical to that of air, resulting in minimal magnetic attenuation. Lately, capacitive coupling has received great interest in wireless power transfer due to DC efficiency at ultra-short distances when long cables are used [43,44]. The most MI antennas are designed at Very Low Frequency (VLF) to maximize the range of operation due to their long wavelength.

A comparison study of efficient small magnetic and electric dipoles was performed in [45] using analytical formulas. In the analysis, shallow water propagation was assumed, where the authors stated that the main propagation path was the air-seawater interface, in which the surface waves play an important role. For the study, a contra-wound toroidal helix antenna (tranverse electric antenna) at 1 kHz displayed greater efficiency than the tranverse magnetic (TM) antenna, exploiting the generated/propagating Zenneck surface waves [45]. When feeding the helical windings around the toroidal core with opposite currents, the net horizontal electric field components cancel out and can be treated as multiple loop TE dipoles.

Different articles discussed and analyzed the near-field communication capabilities of magnetic dipoles. The analysis of magneto-inductive behavior in small loops has traditionally relied on analytical formulations [45] or equivalent circuit models [42], often incorporating transformer representations to account for near-field coupling effects. Nowadays, for more accurate results commercial full-wave EM solvers are preferred for the development of underwater antennas [31]. In [31], a tri-directional coil antenna was proposed consisting of three coils placed perpendicular to each other to produce an omnidirectional pattern independent of the direction of the incoming signals. The tri-directional coil antenna can be used as a sensor for coordinating and maneuvering of underwater robots and vehicles. This requires each robot to be aware of the relative 3D positions of its immediate neighbors as well as the absolute coordinates in the 3D underwater space. However, the use of three antennas significantly increases the volume of the sensor making it difficult to be integrated in a small AUV.

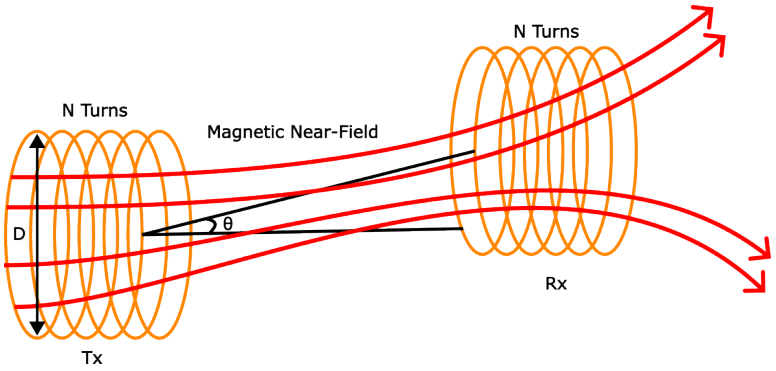

Figure 6. An example of Magnetic Induction communication system for underwater systems.

An evolution of the tri-directional antenna was presented in [41] where a reconfigurable alternative was derived for the excitation of circular polarized magnetic fields. For this reason, magnetic near-field coupling was utilized, functioning as a loosely cou-

pled transformer. The transmitted power decreases proportionally to R^3 for distances shorter than the transmission wavelength, enabling operation within the frequency range of 500–2500 Hz. The numerical models demonstrated that, despite the relatively low conduction losses, the coupling loss remains extremely high, limiting the propagation distance to less than 10 m, with an overall attenuation of approximately 145 dB. Similarly, an MI antenna was designed for communication between air and underwater sensors when the transmitter is 20 m below the surface. The developed small loop inside the water operates at 1 m, in which the radiation resistance is almost zero. However, the transmitting loop is capable of producing $SNR = 50$ dB for 2 kbps data rate based on simulations [46]. In [47], a loop-antenna-based MI communication system was developed, incorporating a non-Foster matching network to enhance channel capacity. The system used Orthogonal Frequency Division Multiplexing (OFDM) to transmit digital images at data rates of up to 50 kbps, depending on the separation between the transmitter and receiver. It achieved ranges of up to 20 m at any ocean depth while operating with less than 10 W of transmit power. The non-Foster matching circuit—a frequency-dependent amplifier—was employed to neutralize the coil's reactive component through active elements, thereby reducing the frequency dependence of the induced current in the loop. Using MI coupling loops with a radius of 15.5 cm, six (6) turns, and operating at 65 kHz, the system achieved robust OFDM-based data exchange resistant to frequency-selective fading.

An experimental study was presented in [48], where a 3.65 m underwater communication link was established using a self-matched three-turn loop antenna operating at 2.95 MHz, enclosed in a waterproof air-filled housing. The enclosed box was used to mitigate the enormous loss induced due to direct contact between the conductive seawater with the metallic conductor. The results indicate an almost linear attenuation of the signal, with a slope of approximately 9 dB/m beyond a 1 m separation between the transmitter and receiver [48]. However, this holds true for a certain range where the near-field is present, after a certain range the attenuation is going to skyrocket when the far-field region is going to start.

A Double-loop antenna operating at 5.5 MHz was employed in [15] as both transmitter and receiver to efficiently excite dipole radiation waves. The authors enclosed the antenna in a distilled water tank to improve impedance matching and reduce near-field losses caused by conductive seawater. The redesigned antenna, referred as *barrel antenna*, employed a parallel-wire transmission line immersed in pure water within a PVC barrel to generate dipole oscillations. The barrel antenna presents a significant enhancement about 40 dB compared to the plain double-loop antenna when emitting into seawater. An experiment was carried out within Weymouth Bay where the propagation of EM for 85 m was verified at a depth of 4 m [15].

2.4. Dipole Antennas

Symmetrical dipole antennas are among the earlier radiating elements, consisting of two metallic rods connected to a voltage source (see Figure 7a). A conventional half-wave dipole has an overall length of $\lambda/2$ and produces a cardioid-shaped radiation pattern in the far field, with a typical gain of 2.15 dBi. Electrical dipoles can operate in either near-field or far-field coupling; however, far-field operation is more commonly utilized, since, as discussed in the previous section, loop antennas generally provide higher efficiency in near-field coupling scenarios. The typical operating frequency of electric dipoles is below 1 MHz, as attenuation becomes excessive at higher frequencies, limiting their effectiveness for long-range coverage [49]. Nevertheless, some recent studies have begun to explore higher-frequency dipoles [50]. In underwater applications, integrating a half-wave dipole into an AUV is impractical due to its large physical size. Therefore, alternative designs of

electrically short dipoles are preferred, with the goal of maximizing efficiency, bandwidth, and gain while maintaining compact dimensions. An example of an electrical short dipole for scuba divers communication was presented in [49], where a $\lambda/25$ dipole was simulated in EM simulator. The electric field generated by the two antennas exhibits strong consistency with the theoretical predictions obtained from the King–Iizuka model [51].

An LF insulated dipole antenna with an appropriate matching network with lumped elements was proposed in [52] operating at 200 kHz for seawater applications. The authors selected to develop a long antenna (200 m) insulated with PTFE to increase the realized gain of the antenna (−61.3 dBi) to compensate for the high-loss seawater environment. However, the enormous length of the antenna makes it impractical for AUVs or generally portable applications.

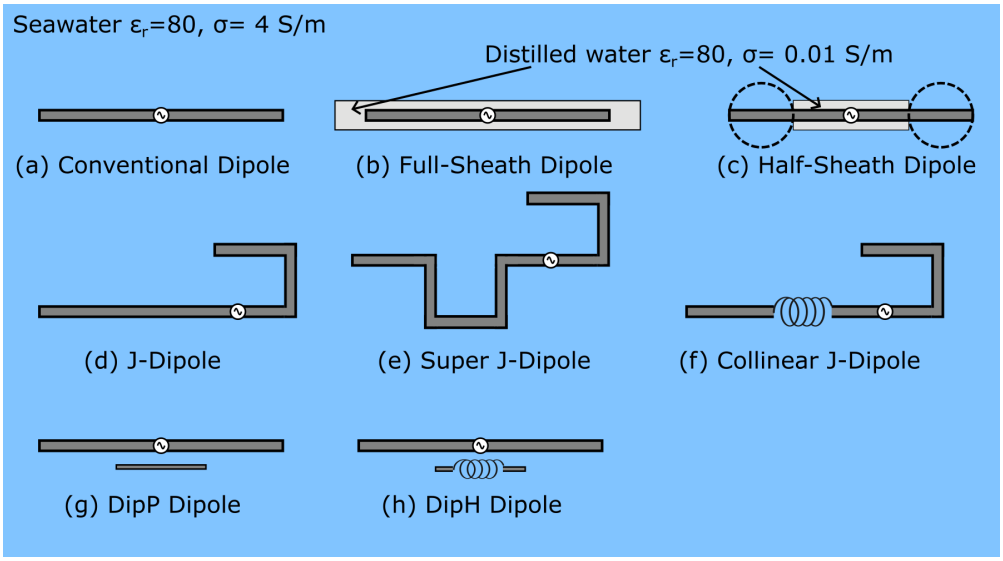

Figure 7. Configurations of (**a**) conventional, (**b**) full-sheath, (**c**) half-sheath, (**d**) J, (**e**) super J, (**f**) collinear J, (**g**) DipD and (**h**) DipH dipole models.

The main challenge faced by a conventional dipole antenna is the low real part of the input impedance making it extremely challenging to match with the microwave source. This is the primary reason for the degraded performance observed in many systems when tested under real-world conditions compared to numerical results [50,53]. In an effort to increase the real part of the impedance, the "sheath" dipole [54] was introduced. Sheath dipoles were proposed as a solution to the current flowing from the antenna conductor that passes through the conductive seawater, completing a loop. As a result, seawater generates a resistive component, while the loop itself contributes an inductive component. In the full-sheath structure (filled with distilled water), as seen in Figure 7b, greater impedance was observed due to small conductivity of distilled water at low frequencies [54]. As the frequency increases, the input impedance behavior begins to resemble that of dipole antennas submerged in freshwater. In the half-sheath dipole (Figure 7c), a distinctive behavior is observed where both the resistance and inductance increase, enabling easier impedance matching with the load. At high frequencies, similar behavior with full sheath dipole is displayed. Based on the results presented in [55], which provide analytical formulas for the impedance and transmission factor of an electrically small half-sheath dipole antenna submerged in seawater, the half-sheath dipole emerges as the optimal solution for near-field links, minimizing the attenuation coefficient. An addition to the half-sheath dipole for seawater application includes the utilization of spherical electrodes (highlighted with dashed lines in Figure 7c). The use of spherical electrodes in dipole antennas is not a recent development; it was first introduced in earlier studies such as [56]. The expression

of the transmission factor presented in [55] demonstrates that reducing impedance leads to a higher transmission factor.As described in [53], increasing the electrode thickness can improve antenna performance by reducing the local electric field intensity and minimizing ohmic losses near the electrode surface. Nevertheless, cylindrical geometries are not always optimal, as the electric field around a charged cylinder tends to be non-uniform, particularly near its edges. To overcome this non-uniformity, the authors in [53] investigated spherical electrodes, as they generate a more uniform electric field, reduce losses, and maximize the transmission factor when the electrode's maximum dimension is fixed. In a field experiment conducted on Ishigaki Island, Okinawa, Japan, the antenna prototype operating at 100 kHz was tested. The results demonstrated an improvement of 5.9 dB in transmission loss compared to a conventional half-sheath dipole, confirming its theoretically predicted higher efficiency.

A notable variation of the conventional dipole antenna is the J-dipole (see Figure 7d), which can be impedance-matched without the need for an external balun (balance-to-unbalance transformer) and provides greater flexibility for installation on various surfaces. The J-pole antenna typically resembles the shape of the letter "J" consisting of a half-wavelength vertical radiator end-fed via a quarter-wavelength matching stub. By adding a phasing stub and an additional half-wavelength vertical section to the basic J-pole, the *super J-pole* configuration is obtained as seen in Figure 7e. Furthermore, replacing the phasing stub with a phasing coil results in the *collinear J-pole* design of Figure 7f.

In free-space conditions, the super J-pole has been demonstrated to exhibit wider bandwidth and higher gain compared to the standard J-pole [57], while the collinear J-pole further enhances the performance of the super J-pole. Experimental analysis in seawater at 40 MHz indicates that the super and collinear J-pole configurations maintain similar bandwidths (approximately 28 MHz), which are reduced compared to air operation due to the higher conductive losses of seawater. Although extremely high values of directivity were observed in simulations, such gains are practically unattainable in seawater environments due to poor radiation efficiency [58]. Nevertheless, the super and collinear J-pole antennas provide higher directivity compared to the standard J-pole design. The increased directivity of the J-pole antenna for both freshwater and seawater applications was highlighted in [59], when compared to conventional loop and dipole antennas. However, its bandwidth and radiation impedance were narrower, indicating that overall efficiency would be limited. An experimental study [60] confirmed the slight improvement of received voltage compared to a similar sized loop antenna at 7 MHz inside a pool filled with seawater. However, the 30 MHz antennas exhibited a similar received voltage, indicating that at lower frequencies the J-dipole achieves better performance than the loop antenna.

A high-frequency example is the design of a wideband dipole antenna capable of receiving/transmitting signals at a center frequency 61.5 MHz with a bandwidth of 10 MHz [50]. The dipoles were fabricated using aluminum duct pipes covered externally with PVC pipe and the final structure was watertight sealed around. The overall communication system includes two software defined radio (SDR), they used to model a 4G LTE network. The antennas were submerged in a fresh water pool using concrete blocks at a distance of 7 m but the system could not establish a reliable connection due to losses.

Aboderin et al. [61] propose the usage of parasitic elements to increase the bandwidth of a dipole antenna for underwater applications. Two different configurations were tested including a dipole antenna with ordinary capacitive parasitic element (DipP) and a dipole antenna with a coil as parasitic element (DipH). The two different structures are shown in Figure 7g and 7h, respectively. An experimental test conducted inside a pool filled with freshwater with conductivity 0.0487 S/m, where the DipH antenna displayed a fractional bandwidth above 150% at a center frequency at 65 MHz. Both antennas were able to

maintain the link, assuming a receiver sensitivity of −90 dBm and a transmitter output power of 10 dBm, the estimated maximum operational range is approximately 7 m at 25 MHz and 6.4 m at 40 MHz [61].

2.5. Directive Antennas for Longer Ranges

The antenna designs previously mentioned primarily focused on maximizing efficiency and maintaining omnidirectional characteristics to effectively cover the surrounding space. However, distributing energy in all directions reduces the operational range of the communication or sensing system. A well-established technique for long-range air/vacuum applications (e.g., satellite communications) is the adoption of highly directive antennas which concentrate the EM energy into a single direction. Adopting this technique comes at the cost of requiring the antenna to be oriented toward a specific direction to establish an efficient communication link. Thus, it may sound rational to compare the use of directive antennas with optical communication systems which can propagate at longer ranges permitting higher data rates. However, directive antennas can be used as a compromise between omnidirectional EM antennas and optical systems because the first can operate at low ranges but supporting all surrounding space while the optical systems achieve greater ranges but with very specific direction. Even small degrees of misalignment between two optical sensors can cause severe degradation of the communication link. Furthermore, optical sensors cannot be used effectively for sensing applications due to the narrow beamwidth of light, which offers high resolution but results in long scanning times. On the other hand, directive antennas present a larger beamwidth (10°–20°) which can provide longer ranges without having problems with misalignment. A highly directional antenna enables the WLAN Access Point (AP) to focus its signal toward a specific target area. By concentrating the transmission toward regions with high user density, it becomes possible to extend wireless coverage efficiently. This approach provides an efficient and practical solution for improving network accessibility in densely populated areas, eliminating the need for deploying additional APs.

The major challenge in designing directive antennas lies in their large physical dimensions and suboptimal performance, that primarily results from the complex near-field effects [15,16]. The signal is too weak to propagate into the far-field region, making it impossible to define the antenna "Gain". Consequently, the literature contains only a limited number of studies exploring the potential use of directive antennas or antenna arrays. For arrays, the dominance of near-field effects prevents the constructive interference essential for their operation, as demonstrated in [62], where various configurations of arrays employing bicone and bow-tie elements were simulated, revealing low gains in the far-field. An additional reason related to this is the small inter-element distance due to space constraints inducing currents between the neighboring elements. The challenge in developing antenna arrays inside sea water is an inherent feature, due to its very high losses. Explicitly, antenna arrays employ directional beams based on constructive interference of waves generated by each antenna element. The excessively high losses in seawater environment do not allow the existence of strong enough waves at distances where this summation is expected to occur.

Helical antennas have been investigated as a directive alternative to MI loop antennas for far-field communication. These antennas exhibit wideband characteristics, consisting of multiple loops similar to the MI loop sensors described in Section 2.3. The key distinction lies in their operating mode: MI loop antennas are designed to maximize near-field coupling (normal mode), whereas helical antennas are optimized for far-field radiation (axial mode) [63]. A helical antenna operating in axial mode was tested inside a PET container with various buffer materials, as illustrated in Figure 8. The study concluded that distilled

water environment provided the best gain performance. Furthermore, a helical antenna operating at 433 MHz (ISM band) was fabricated and experimentally validated, achieving a communication link of up to 3 m [63].

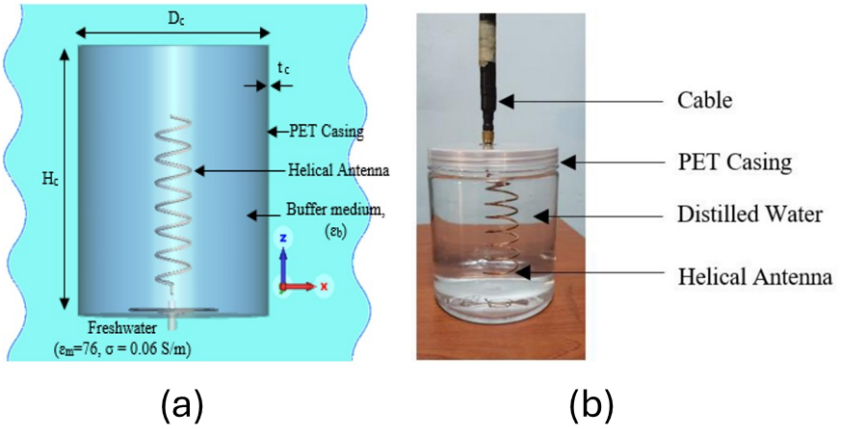

Figure 8. (**a**) The axial mode helical antenna structure and the (**b**) Fabricated prototype in Distilled Water and PET Container [63].

An Orbital Angular Momentum (OAM) dielectric loaded horn antenna was proposed for underwater communication link in [64]. The antenna was designed to operate at 2.5 GHz with a novel distilled water-filled coaxial impedance matching circuit. Dielectric loading was employed to provide impedance matching and mechanical robustness for the feeding probe, utilizing zirconium oxide (ZrO_2) with a dielectric constant (ϵ_r) of 36. For the experimental study, deionized water was used as the buffer medium. For the generation of an OAM system multiple single elements were placed in a circular manner (Uniform Circular Array) and an appropriate phase shift was applied in each element. Orbital Angular Momentum is characterized as a vortex wave which displays a rotating phase factor defined by an integer number called "topological charge". The significant benefit of OAM modes is their ability to span a Hilbert space of infinite dimensions, providing a novel degree of freedom to increase communication capacity and to improve imaging resolution, respectively. The capability of supporting OAM modes was verified, but the transmission losses due to conductive sea water are tremendous even for a gain of 13.5 dB at 2.5 GHz. Furthermore, the uniform circular antenna occupies a significant amount of space, making it impractical to integrate into compact ROVs or AUVs.

A similar case of an OAM system based on broadband ridge horn antennas was investigated in [65] for a 2D underwater imaging system. The configuration of the overall system where the horn antennas are used as a circular array along with its S-parameters is presented in Figure 9. The verification of the system's operation was carried out using as targets two corner reflectors, the result shows that the targets can be distinguished efficiently. However, the measured radiation pattern differs from the simulated due to different loss of water in the simulation and experiment, the weak signal detection errors, the reflection of some measuring devices and the spatial averaging effect of measured data caused by the finite size of receiving antenna. However, that type of antenna cannot be used efficiently for communication links attributed to the short-ranges which can be provided.

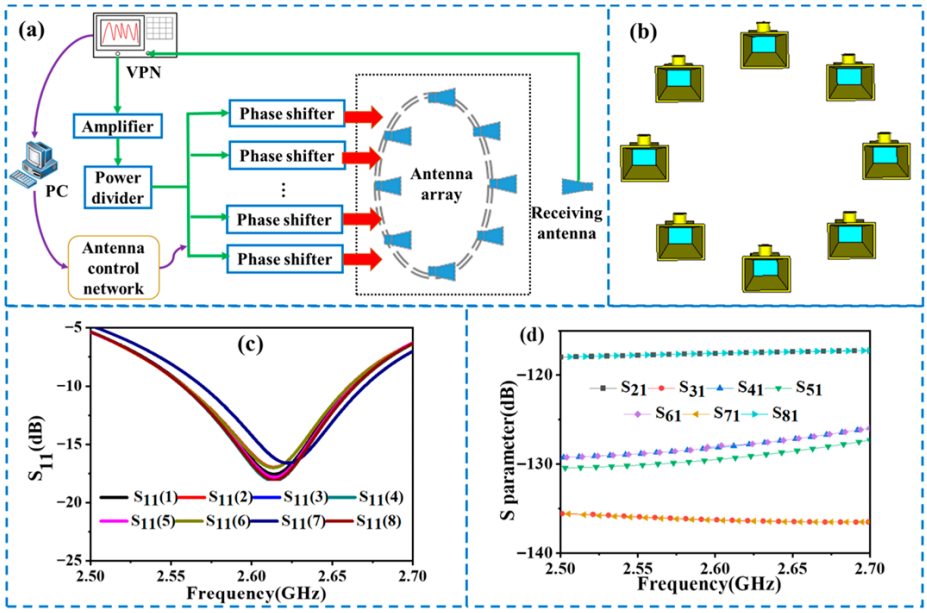

Figure 9. (**a**) Schematic configuration for generating OAM beams in water; (**b**) geometry of the OAM horn antenna array; (**c**) S_{11} of eight elements; (**d**) S parameters between the first element and the others [65].

2.6. Magnetoelectric and Mechanical Antennas

Conventional long-wave antennas must be physically large to operate efficiently at low frequencies, that makes them difficult to transport, deploy, and maintain. In contrast, mechanical antennas generate electromagnetic radiation through mechanical vibrations that induce electric or magnetic dipole transitions within the material, thereby overcoming the size and efficiency limitations of conventional designs and enabling substantial miniaturization. Magnetoelectric and other mechanical antenna technologies have therefore become attractive candidates for very low-frequency (VLF) applications, especially where compact form factors and high operational efficiency are required. It is important to recognize that the frequency of VLF electromagnetic waves falls between 3 and 30 kHz, corresponding to free space wavelengths that extend from 10 to 100 km. Due to its large skin depth and strong dielectric penetration ability, VLF has become an attractive solution. However, the emission capability of the currently available compact antennas is constrained at these low-frequency ranges owing to their limited electrical dimensions. Even the most advanced electrically small antennas find it difficult to simultaneously achieve a combination of small size and high radiation efficiency constrained by the Chu–Harrington limit.

The benefits of such antennas are highlighted in the cases of highly conductive media, such as seawater or human tissues [66], due to the immunity of the magnetic field to the lossy dielectric material. Exploiting the magnetoelectric (ME) coupling and the electromechanical resonance (EMR), mechanical antennas overcome several limitations associated with conventional electric current induced antennas. Unlike metallic antennas, which radiate based on electromagnetic properties, ME antennas resonate through the acoustic characteristics of their physical dimensions, as illustrated in Figure 10. This allows for a significant reduction in antenna size without compromising radiation performance and efficiency. Composite ME and multiferroic materials combine the beneficial properties of ferroelectrics and ferrites. These materials operate on the principle of magnetoelectric coupling, which enables modification of their magnetic properties through the application of an external electric field. The mechanism begins when an electric field is applied to a piezoelectric material, causing the microscopic electric dipoles to shift, resulting in mechanical deformation. This elastic deformation is transferred to the magnetic material at the

interface, where it triggers the effects of magnetostriction or piezomagnetism, leading to macroscopic magnetization. In ME antennas, a low-frequency alternating magnetic field (H_{AC}) interacts with a magnetostrictive layer, causing magnetic domains to rotate and shift, generating mechanical deformation. The strain is transferred to an acoustically coupled piezoelectric layer, inducing electrical polarization or the reverse process depending on the mode of operation. The result is an antenna capable of operating at resonant wavelengths up to 10^5 times smaller than traditional electric-field-based antennas, making them highly advantageous for miniaturization and efficiency. The electromagnetic radiation of the magnetoelectric composite material originates from magnetization oscillations within the magnetostrictive layer. Positioned between a pair of magnetostrictive layers (see Figure 10), the contribution of the piezoelectric layer to electromagnetic emission is often considered negligible. In contrast, the radiation pattern of the magnetostrictive layer closely resembles that of a perfect magnetic dipole. Common piezoelectric materials include PZT, barium strontium titanate (BST), and lithium niobate, while magnetostrictive materials include yttrium iron garnet (YIG), Terfenol, Metglas, nickel ferrite (NFO), and Galfenol. These materials play a crucial role in enhancing the performance of various devices. ME antennas have emerged as an effective solution for antenna miniaturization. In recent years, the adoption of ME antennas for communication in both atmospheric and underwater environments has been experimentally validated [67].

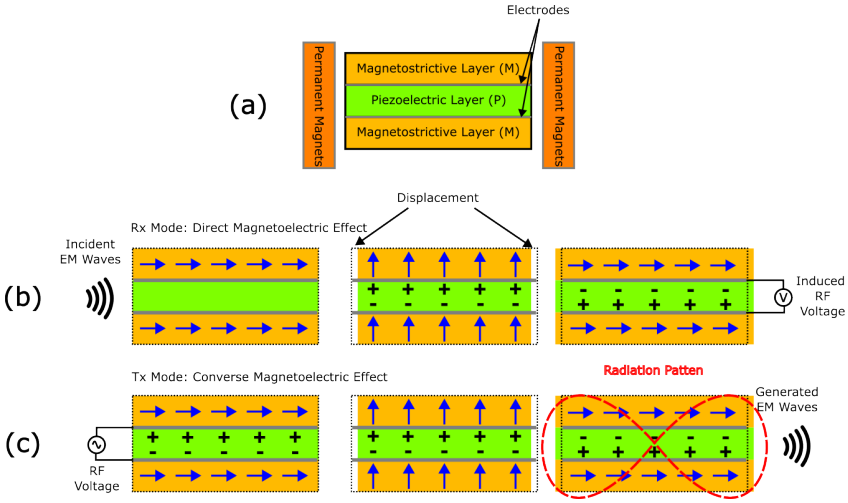

Figure 10. Basic principle of magnetoelectric antenna's electromechanical resonance where (**a**) is tri-layer structure, (**b**) receiving and (**c**) transmitting mode.

One of the key features of ME antennas is their real resonant impedance, which distinguishes them from electrically small antennas of comparable size that exhibit high reactance. A high real input impedance enables the antenna to accept and radiate substantial amounts of power, whereas high reactance leads to power reflection. This characteristic improves overall power transmission and efficiency, making LF ME antennas a superior alternative to traditional EM antennas, particularly for underwater and other challenging environments. However, it is important to note that the input impedance of submerged ME antennas in water has not yet been reported in the literature, although some studies have verified their underwater operation [68,69]. Additionally, ME antennas offer the advantage of dual functionality, enabling both wireless energy harvesting and sensing at different frequencies. This makes them more versatile, extending their utility beyond data transmission to applications such as environmental monitoring and energy-efficient systems. Despite the fact that the radiation efficiency of these antennas may not always surpass conventional antennas in absolute terms, their ability to achieve acceptable efficiency (0.5%) at significantly smaller sizes remains a considerable advantage, particularly in resource-constrained environments

(e.g., underwater communication networks based on small AUVs). However, the efficiency of these acoustically driven antennas depends largely on their specific design and implementation. While impedance characteristics contribute to improved matching and overall performance, the radiation efficiency is strongly influenced by the fabrication techniques and structural design of the antenna. As research progresses, further optimization in this area could unlock even more potential for ME antennas in underwater communication and other low-frequency applications.

Although the popularity of magnetoelectric antennas for low frequency applications (mining operations, biomedical devices, ground penetration Radar etc.) [66,67,70], there is a gap for underwater applications. Du et al. [71] presented a novel acoustically actuated ME antenna based on EMR for very low frequency (VLF) underwater communication networks. A tri-layer sandwiched structure, consisting of magnetostrictive–piezoelectric–magnetostrictive (M–P–M) layers, operates in the longitudinal–transversal mode to maximize radiation efficiency. The symmetric MPM structure counterbalances the vibration noise generated in the M-layer to improve the ME response intensity, which has been widely used in ME devices. An underwater communication range of approximately 0.26 m was measured at a moderate data rate of 100 bps with low power consumption of 0.147 W. ME antenna can match more easily the characteristic impedance due to their small reactive part. However, to improve system performance, future efforts should focus on optimizing the material properties and structural design of ME antennas to enhance VLF signal transmission and reduce the reflection coefficient, which is currently extremely high ($|S_{11}| > -0.8$ dB), thereby decreasing antenna efficiency. In experimental tests, the system was submerged in tap water, achieving a detection range of 2.2 m before reaching the sensitivity threshold. The signal decay was observed to be slower than the $1/R^3$ rate typical of EM wave propagation, with additional multipath components—such as surface reflections, floor reflections, and water-to-air boundary reflections—contributing to the received signal, as illustrated in Figure 3.

A similar three-layered (MPM) structure consisting of PZT-5H and FeBSiC (see Figure 11a) was proposed in [68] operating at 14.1 kHz. Since the piezomagnetic coefficient of all magnetostrictive materials is almost 0 under zero magnetic field, for that reason it is necessary to integrate a DC bias magnetic field using permanent magnets. An experimental study was conducted with a modulated signal with 2-ASK (Amplitude Shift Keying) when the ME antenna submerged in a seawater-filled tank with $\sigma = 5$ S/m (Figure 11). A data-rate of 200 bps was achieved for a distance of 1 m, including 0.7 m in air and 0.3 m underwater environment, when the transmitted antenna is positioned outside the water tank to model a communication link between air-water systems. Another symmetric MPM structure was studied in [69] based on a sandwich-structured Terfenol-D/PZT/Terfenol-D ME antenna with 91.8 kHz frequency for bidirectional communication in a saline environment with the conductivity of 5 S/m, with near field performance close to the magnetic dipole antenna. To ensure seamless operation, an integration scheme was introduced based on a rubidium magnet to generate the required magnetic field. However, the measured reflection coefficient remained insufficient ($|S_{11}| > -2$ dB), limiting the antenna's capabilities. ASK modulation was employed for effective transmission over a distance of 30 cm underwater. In the same setup, the ME antenna underperformed compared to a conventional loop antenna, achieving approximately 3.6 times lower normalized radiated power [69]. The antenna efficiency was estimated to be around 2.23×10^{-16}.

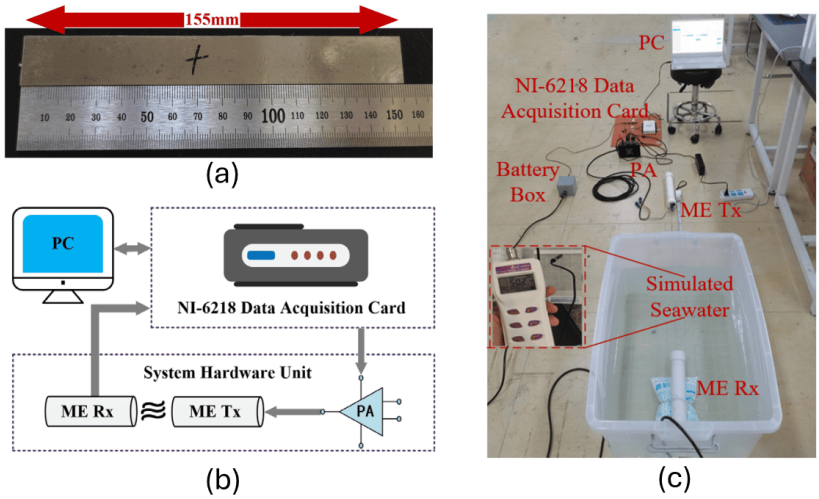

Figure 11. (**a**) Fabricated three-layered (MPM) ME antenna, (**b**) schematic of experimental setup and (**c**) photo of receiving and transmitting test system in seawater.

A major limitation is the narrow operating bandwidth caused by the high quality factor (Q) of these resonators. For example, a Q value of 632 results in a fractional bandwidth of only 0.228% [72]. Broadening the bandwidth can be achieved by introducing materials with higher mechanical losses, such as AlScN or ZnO, to lower the device's intrinsic Q_{loss}. However, this approach risks degrading radiation efficiency unless the radiation Q_{rad} is simultaneously reduced. Alternatively, bandwidth can be improved by designing arrays where individual resonators feature varying thicknesses.

2.7. Compact Patch Antennas

As described in Section 2.2, miniaturization is a fundamental characteristic of the novel underwater antenna capable of mounting on AUVs. The magnetoeletric antenna seems to be a good solution regarding its compact size, but due to its limited research effort and its low power handling capabilities, printed planar antennas began to draw more attention due to their attractive features. Their low-profile and lightweight structure make them ideal for integration into small platforms such as AUVs and ROVs. They are cost-effective and suitable for mass production due to their compatibility with standard PCB fabrication techniques. Additionally, planar and generally printed antennas support versatile designs, enabling multi-band and wideband performance while maintaining mechanical robustness and ease of deployment. Patch antennas, particularly when implemented as printed arrays, are capable of producing high-gain beams to compensate for conduction losses, while broader bandwidths can be achieved through the use of appropriate parasitic elements. Microstrip antennas are widely recognized for their mechanical robustness, low manufacturing cost, and compatibility with Monolithic Microwave Integrated Circuit (MMIC) technologies. They are also lightweight, compact, and offer design flexibility, including frequency tunability. Despite these advantages, microstrip antennas exhibit certain limitations, such as relatively low efficiency due to dielectric substrate and conductor losses, limited power-handling capability, unwanted feed radiation, and inherently narrow bandwidth.

The most challenging part of designing a patch antenna for underwater communication is their size. In contrast to previously discussed antenna configurations, which can be submerged in water or in a buffer medium, patch antennas are printed on a substrate. Thus, the operation frequency range is determined from the dimensions of the printed patch and the characteristics of the substrate layer (dielectric constant and thickness). Considering that, a patch antenna will be designed using the same approach for both air and underwater applications, under the assumption that the antenna will not be in direct contact with water

or any buffer medium, which is a common practice. For that reason, most underwater patch antennas operate at frequencies above 100 MHz. The response of a patch antenna at 2.45 GHz submerged in different types of water (tap water, mineral water, seawater and fountain water) was investigated in [73]. The results show poor matching due to the presence of water, which nullifies the radiation capabilities of the antenna.

An underwater microstrip antenna array was investigated in [74] to enhance electromagnetic radiation performance by leveraging wave propagation through the sea surface. A circular microstrip patch antenna was used due to its compact structure and ease of integration. The array was placed in a shallow water environment with the goal of maximizing radiation through the sea-air boundary. The design takes into account the high permittivity and conductivity of seawater, which significantly affect the radiation pattern and impedance matching. Simulation results demonstrate that careful positioning and design of the microstrip array can lead to meaningful radiation above the sea surface, offering a feasible approach for short-range underwater-to-air communication. The simulations show that seawater can be used as the medium layer of the uniform microstrip array to generate an energy distribution in a near region similar to that of the conventional microstrip antenna. Furthermore, the element spacing for the underwater array should be adjusted based on practical application.

A circular patch antenna with a buffer layer was designed in [75] for high-data-rate underwater applications. This study introduced the use of a buffer layer as an impedance-matching interface between the radiating antenna and surrounding water, aiming to improve overall antenna performance. Simulations indicated optimal results when the buffer material's dielectric constant was set to the geometric mean of those of air and the transmission medium, and when the buffer thickness corresponded to the near-field region of the antenna. This follows the classical impedance-matching approach, requiring the buffer layer to be a quarter of the guided wavelength ($\lambda_g/4$). These findings were experimentally validated using a circular patch antenna with a partial ground plane, tested in a tap-water-filled tank, as seen in Figure 12. The authors employed a partial ground technique with an etched slot to enhance bandwidth, at the expense of generating a back lobe. The buffer layer was fabricated in-house by combining water and methyl acetate. In this configuration, the buffer completely encapsulates the antenna, which may limit its practicality for real-world deployment. Furthermore, the study did not investigate the radiation characteristics of the antenna.

A widely used printed antenna structure for underwater applications is the bow-tie antenna. Recognized for its structural simplicity and wideband performance, the bow-tie antenna can be viewed as a planar adaptation of the bi-conical dipole (Figure 13a). The Bicone Antenna, characterized by two conical conductors aligned along a common axis and joined at their vertices, is an omnidirectional broadband antenna offering wide bandwidth and uniform radiation—crucial features for high data rate underwater communication. Its broad coverage and low return loss make it an effective solution for platforms such as ROVs and AUVs. It offers several key advantages, including low fabrication cost, high radiation efficiency, ease of manufacturing, and a compact, low-profile design. In [76], a bow-tie antenna backed by a ground reflector (Figure 13b) was investigated for underwater Wi-Fi communication at 2.45 GHz. The integration of a ground reflector significantly improved the antenna's performance stability, making it less sensitive to small variations of the design parameters and thereby enhancing robustness against manufacturing tolerances. Two antenna configurations—one with and one without an insulating coating—were experimentally tested in a freshwater plastic tank. The results demonstrated sufficient received signal strength to establish a communication link up to 55 cm. Beyond this range,

the Received Signal Strength Indicator (RSSI) dropped sharply below the noise floor, a behavior attributed to multiple internal reflections within the tank environment.

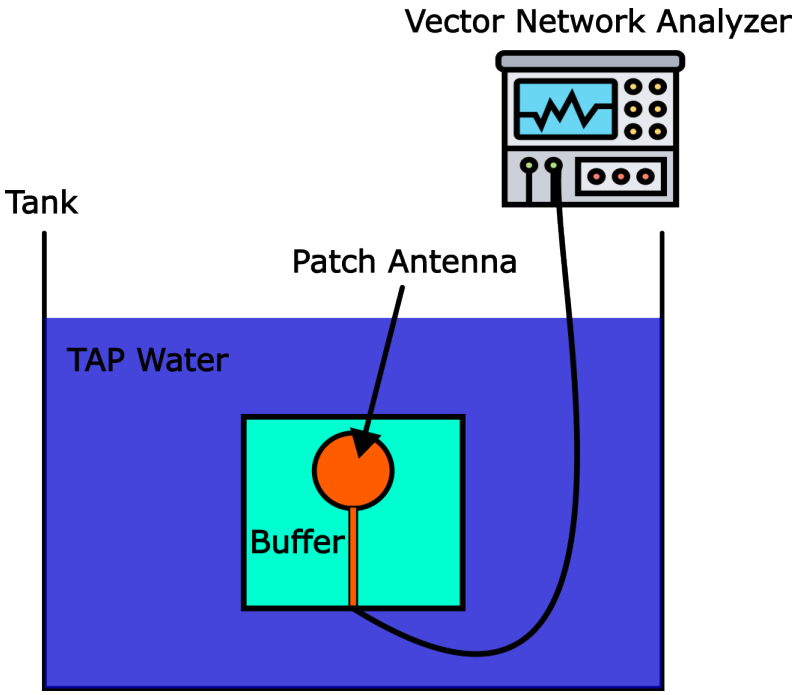

Figure 12. Illustration of S_{11} measurement setup of circular antenna as conducted in [75].

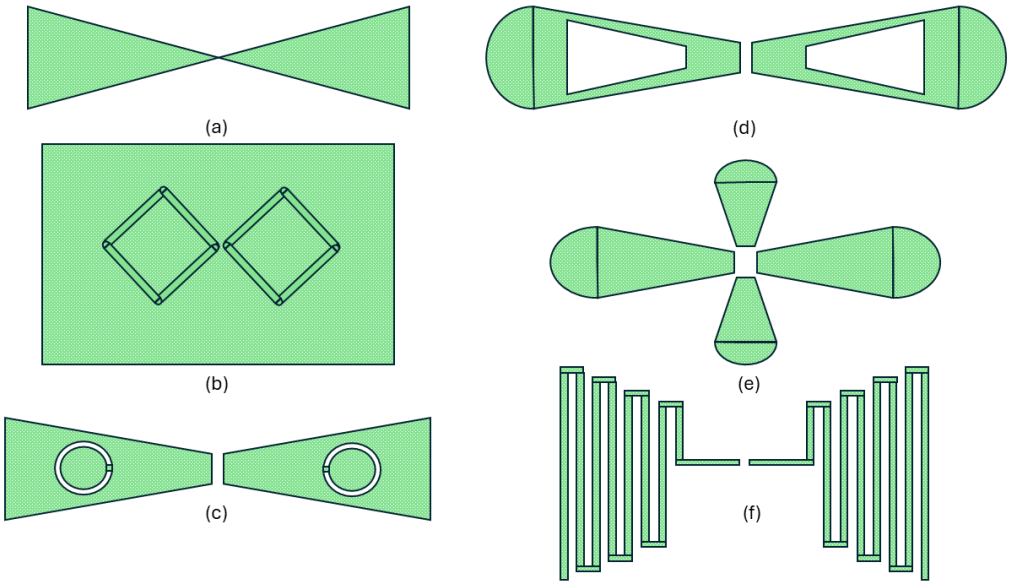

Figure 13. Configurations of (**a**) conventional, (**b**) ground-backed [76], (**c**) arc-shaped circular slots [77], (**d**) RBTA with slot [62], (**e**) quad taper [78] and (**f**) meander [79] bow-tie antennas.

An alternative bow-tie antenna was proposed to operate at 2.4 GHz and 5.1 GHz, corresponding to the IEEE 802.11b/g/n standards for WLAN communications [77]. The antenna, featuring arc-shaped circular slots and occupying a surface area of only 1.4 cm^2, as shown in Figure 13c, was implemented to mitigate path loss in water with non-zero conductivity. Fabricated on a bi-triangular sheet of Duroid substrate, the antenna demonstrates a measured gain of 1.2 dBi. The operation of the antenna was verified in a pool filled with seawater with 3.1% salinity ($\sigma = 50$ mS/m) where a prefabricated remote controlled vehicle was utilized for the testes. The received power ranged between -64 dBm and

−71 dBm. These results indicate that, although the signal becomes less stable due to the conductive nature of the medium, a satisfactory communication link can still be maintained to seawater conditions.

An analysis of the communication capabilities of antennas operating at 900 MHz (ISM band) in different water types was presented in [62]. The study evaluated the performance of the Rounded-Edge Bow-Tie Antenna (RBTA), including a mid-sliced variation, both individually and in an array configuration, as illustrated in Figure 13d. The RBTA was designed to improve radiation characteristics, of the conventional bow-tie antenna, by minimizing sharp-edge effects. This geometric refinement leads to a smoother current distribution, enhanced impedance matching, and increased bandwidth—features that make it highly suitable for short-range underwater communication. An additional modification, involving a sliced structure at the antenna's midpoint, was introduced to improve impedance matching and radiation efficiency. Experimental results demonstrated that RBTA performs effectively in underwater environments, with its performance strongly influenced by the dielectric properties of the surrounding medium (air, freshwater, seawater). The choice of 900 MHz introduces challenges in seawater, where high conductivity leads to substantial signal attenuation. Performance comparisons across different media revealed the significant impact of the underwater environment on antenna behavior. In air, the antenna exhibited a maximum gain of 2.3 dB. Immersion in freshwater resulted in a reduced gain of −2.2 dB due to changes in the electromagnetic properties ($\epsilon_r = 81$ and $\sigma = 0.05$ S/m) of the surrounding medium, which affects the radiation efficiency. In seawater, the antenna performance degraded further, with a measured gain of −11.9 dB, primarily due to the medium's high conductivity ($\sigma = 4$ S/m) and the associated signal attenuation. These results underscore the severe constraints imposed by underwater environments, particularly in saline conditions.

Two recent studies have focused on the design of wideband bow-tie antennas for underwater applications [78,79]. In [78], a multiband bow-tie patch antenna with circular insulation (RT duroid) and varied tapering (Figure 13e) was proposed, generating an omnidirectional radiation pattern and achieving impedance matching over the frequency range of 0.5 to 5.2 GHz—corresponding to a fractional bandwidth greater than 1.7. For dielectric insulation and mechanical stabilization, an air-RT Duroid sphere was incorporated as a central support element within the circular configuration of the proposed antenna. The inner surfaces of all taper sections are in direct contact with the sphere, thereby imparting structural rigidity to the antenna and enhancing its resilience under high-tide environmental conditions. This wide operational bandwidth enables improved radiation efficiency and enhanced data transmission rates, making the antenna suitable for underwater sensor network applications. The design improvements included bending the corners of the triangular patches on both sides of the antenna. This modification enhanced the electric field distribution, thereby increasing the overall bandwidth. The antenna dimensions were carefully optimized to maximize radiation efficiency and operational bandwidth. A layer of RT Duroid was employed as the insulating material, facilitating effective energy radiation from the antenna while minimizing strong near-field coupling. In a complementary study, the authors of [79] proposed a novel ultra-wideband (UWB) bow-tie antenna incorporating meander lines, printed on a single-sided dielectric substrate, as shown in Figure 13f. This design demonstrated excellent reflection coefficient, far-field performance, and current distribution characteristics across a wide frequency range of 0.1 to 3 GHz. The antenna was simulated in four different propagation media (Salty seawater, pure water, Red seawater and Arctic Ocean water) with varying conductivities ($\sigma_{salty} = 5.3$ S/m, $\sigma_{pure} = 0$ S/m, $\sigma_{Red} = 8$ S/m and $\sigma_{arctic} = 2$ S/m), while maintaining fixed physical dimensions and flare angles. It exhibited a dipole-like radiation pattern and retained compactness through the use of the meander line technique, which increases the effective

electrical length without increasing the overall size. These characteristics make the proposed antenna a strong candidate for low-frequency underwater communication systems.

2.8. Discussion-Challenges-Future Aspects

2.8.1. On Antennas Application in AUVs

Following the analysis of potential candidates for seawater underwater antennas, we are going to delve into their practical integration within AUVs and ROVs. As illustrated in Table 2, which summarizes most of the presented antennas, frequency selection is a critical design parameter. Based on the findings in Section 2.1, the operating frequency must remain as low as possible to minimize propagation losses (due to the rapid attenuation caused by the high conductivity of seawater) and provides communication or sensing over at least short ranges. However, implementing efficient low-frequency antennas on small-scale AUVs presents a significant physical challenge due to the prohibiting size of the required radiating elements relative to the vehicle's hull. Consequently, center frequencies above 10 MHz generally preclude links exceeding a few meters. The primary practical application of such high frequencies is communication within an AUV swarm, where individual units act as relays, as proposed in [12]. In this configuration, compact antennas with sufficient bandwidth can be realized to support the data rates required for larger data packages (such as video). Consequently, coordination among AUVs can be achieved with high data rates, which are crucial for applications such as seabed mining and exploration.

For applications operating above 100 MHz, patch antennas emerge as the most suitable candidates, offering wide bandwidth, higher directivity, and a compact quasi-2D form factor that enables conformal mounting to the hull, thereby minimizing hydrodynamic drag. However, the utility of these antennas is limited to extremely short-range links; at such frequencies, electromagnetic waves experience severe attenuation due to the high conductivity of seawater, rather than intrinsic antenna inefficiency alone. As summarized in Table 2, alternative antenna architectures are generally less attractive due to constraints related to size, data rate, or efficiency. In terms of physical dimensions, MI solutions are often impractical for compact AUVs is attributed to the substantial volume required by the coil structures. Furthermore, MI system performance is highly sensitive to the relative orientation of the transmitter and receiver; even moderate misalignment can drastically reduce the magnetic coupling coefficient, necessitating precise coordination between vehicles. Dipole antennas present similar integration challenges. Although their high aspect ratio will permit placement along the external chassis, any protrusion disrupts the hydrodynamic profile of AUV. To mitigate this issue, a fin-like antenna structure—similar to those employed in automotive applications—could be implemented as a monopole using the AUV chassis as a ground plane. Nevertheless, both MI coils and electrically short wire antennas inherently suffer from narrow bandwidths, which limit achievable data rates, as well as poor radiation efficiency. While alternative designs, such as the J-pole antenna, may offer improved bandwidth, they introduce additional structural complexity that complicates mechanical integration into the AUV.

A critical challenge in the design of underwater antennas is optimizing their overall efficiency, which is governed by two primary factors: impedance matching to the source and radiation efficiency. Impedance matching is determined by the reflection coefficient at the feed point, arising from differences between the source and antenna impedance. An antenna's input impedance is heavily dependent not only on its geometry and electrical size but also on the EM properties of the surrounding medium. If an antenna is housed within an air-filled protective radome to prevent galvanic corrosion and eddy currents, the abrupt interface between the air ($\epsilon_r \approx 1$) and the seawater ($\epsilon_r \approx 81$) creates a severe impedance

mismatch. This results in significant signal reflection at the boundary, manifesting as a poor voltage standing wave ratio (VSWR).

Table 2. Summary of Underwater antennas.

Ref.	Type of Element	Size (cm^3)	Freq. (kHz)	BW (kHz)	Direct. (dBi)	Efficiency	Conduct. (S/m)	Op. Range (m)
[45]	Toroid	125,663	1	N/A	N/A	N/A	4	100
[41]	tri-directional loop	1000	1.5	N/A	N/A	N/A	4	10
[46]	Loop Spherical Array	27,000	0.65	0.7	12.5	10^{-9}	3.61	50
[47]	Circular Loop	6	65	N/A	N/A	N/A	4.5	20
[48]	Square Loop	46,440	2950	N/A	N/A	N/A	0.0223	3.65
[15]	Parallel Wire	81,546	10,000	40,000	N/A	N/A	4	85
[52]	Dipole	9×10^9	200	20	2.15	10^{-6}	3.53	N/A
[50]	Wideband Dipole	10,600	61,500	10,000	N/A	N/A	N/A	Failed
[55]	Sheath-Dipole	0.0255	2500	5000	N/A	N/A	4	1
[53]	Sheath-Dipole with Electrodes	6283	N/A	N/A	N/A	N/A	5.1	2.75
[58]	J-dipole	88.8	40,000	27,920	14.05	N/A	4	N/A
[58]	Super J-dipole	63.3	40,000	28,320	25.81	N/A	4	N/A
[58]	Collinear J-dipole	74.2	40,000	28,450	19.52	N/A	4	N/A
[61]	Parasitic P Dipole	356	42,000	65,000	12.5	N/A	4	N/A
[61]	Parasitic H Dipole	981	42,000	74,000	9.92	N/A	4	N/A
[63]	Helical	981	433,000	30,000	19.5	N/A	0.06	3
[64]	Horn Array	472.9	2,620,000	130,000	8	N/A	1.42	0.2
[71]	Magnetoelectric	0.06	22.23	0.06	N/A	N/A	0.0677	2
[68]	Magnetoelectric	0.0465	14.1	0.2	N/A	N/A	5.02	1
[69]	Magnetoelectric	0.00126	91.8	0.1	N/A	2.23×10^{-16}	5	3
[73]	Patch	75	2,070,000	50,000	N/A	N/A	N/A	N/A
[74]	Patch	705,600	12	N/A	N/A	N/A	N/A	100
[75]	Circular Monopole	23,772	450,000	400,000	N/A	N/A	N/A	N/A
[76]	Bow-Tie	9	2,450,000	600,000	N/A	N/A	0.05	0.65
[77]	Bow-Tie	4.2	2,400,000	480,000	1.2	N/A	5.6	0.152
[78]	Rounded Bow-tie	15	1,000,000	1,665,000	3	N/A	0.05	N/A
[79]	Meandered Bow-Tie	0.56	1,120,000	2,900,000	1.2	N/A	8	N/A

To mitigate this, researchers have proposed submerging the antenna in a "buffer" medium [15,54,63,64,75]. By utilizing a dielectric buffer—typically distilled or deionized water [15], or a material with a permittivity intermediate between air and seawater [63]—the radiated waves can be generated within a lossless environment before transitioning into the seawater. A particularly effective approach is encapsulating the antenna in distilled water, which matches the dielectric constant of seawater but exhibits negligible conductivity. This isolates the antenna's reactive near-field from the conductive lossy seawater, thereby minimizing ohmic dissipation while maintaining impedance continuity. Consequently, a robust fabrication strategy requires a compact, liquid-filled sealed enclosure that maximizes matching and prevents direct seawater contact, while facilitating reliable RF and electronic interconnects.

The second limiting factor is radiation efficiency, which is linked to the antenna's physical size and field distribution. The fundamental trade-off between an antenna's electrical size and its maximum achievable efficiency/bandwidth is governed by the Chu–Harrington limit [80]. For low-frequency applications, the requirement for miniaturization typically necessitates a severe sacrifice in efficiency. As introduced in Section 2.6, ME antennas offer a compelling alternative by exploiting mechanical (acoustic) resonance. This mechanism allows the antenna to resonate at much lower frequencies than conventional electrical antennas of comparable dimensions. However, the radiation efficiency of ME antennas is often compromised by weak electromechanical coupling, with reported coupling coefficients frequently below 5% [72,81].

While surveys indicate that the absolute radiation efficiency of ME antennas can be lower than 10^{-7} [82], suggesting they cannot universally replace conventional antennas, they offer distinct advantages in size-constrained, low-frequency applications where they

approach the theoretical performance bounds defined by the Chu–Harrington limit [83]. Furthermore, ME antennas are particularly advantageous when integrated as planar structures near a conductive ground plane (e.g., an AUV hull). At electrically small separation distances (<0.00001λ_g), conventional electric antennas suffer from gain degradation due to destructive interference from image currents. mainly due to the dipole being shorted. In contrast, ME antennas behave as magnetic dipoles, inducing parallel image currents that result in constructive interference and gain enhancement [84]. Therefore, to derive accurate performance benchmarks, ME antennas must be compared against equivalent magnetic antennas (such as loops). As detailed in Table 3, the ME antenna consistently outperforms the conventional loop antenna by at least 15 dB in these scenarios.

Table 3. Comparison of ME and Loop antennas regarding their efficiency ratio (η_{ME}/η_{loop}) and ME gain.

Antenna Description	Size (mm^3)	Frequency (kHz)	Eff. Ratio (dB)	ME Gain (dB)	Ref.
Metglas/PZT/Metglas	640	28.17	37.4	N/A	[85]
PZT/Terfenol-D	4742	37.95	27.23	−165	[86]
Dual Driven ME	28,125	29.46	47	N/A	[87]
PZT/Terfenol-D	2644	35.6	17	−158	[88]
AlN/FeGaB	12.5×10^{-6}	2.47×10^{6}	20.5	−63.5	[89]
AlN/FeGaB	5×10^{-6}	2.2×10^{6}	15	−44.9	[90]

However, the fabrication and operational deployment of ME antennas present significant challenges. The realization of high-performance ME devices is hindered by critical material synthesis and processing constraints. A primary difficulty lies in engineering a rigid, high-quality interface between disparate thin films—typically magnetostrictive metals (e.g., FeGaB or Metglas) and piezoelectric ceramics (e.g., AlN or PZT). Since the device relies fundamentally on efficient strain transfer, any interface defects, lattice mismatches, or poor adhesion will severely degrade the electromechanical coupling coefficient [91]. Furthermore, process compatibility poses a significant hurdle; the high thermal budgets required to optimize the crystallinity of the piezoelectric layer often induce deleterious effects such as oxidation, residual stress, or phase degradation in the magnetic layer, particularly when specific magnetic anisotropies must be preserved [92]. Additionally, for polymer-based nanocomposites (e.g., magnetic nanoparticles embedded in PVDF), preventing particle agglomeration during the curing process is critical to ensuring uniform dispersion and minimizing dielectric losses. Finally, fabricating these devices at the operational NEMS/MEMS scale necessitates complex release steps to define suspended vibrating structures, a process often plagued by mechanical fragility and low yield [93,94].

In conclusion, despite their potential, current ME antennas face barriers to practical deployment, primarily due to insufficient gain and radiation efficiency. To address these limitations, researchers have proposed the implementation of densely packed arrays of ME elements [91]. Unlike conventional electromagnetic antenna arrays, which typically require half-wavelength ($\lambda/2$) spacing to avoid mutual coupling, ME arrays—operating on acoustic resonance principles—benefit from a significantly more compact footprint. Studies on three-element ME arrays indicate that this configuration increases the effective number of magnetic dipoles, resulting in a threefold enhancement of the induced output voltage [95]. Consequently, establishing similar array-based architectures specifically optimized for the underwater acoustic-magnetic environment is a critical direction for future research. A comparison table containing the benefits and drawbacks of each studied antenna type is presented in Table 4.

Table 4. Comparison of Antenna Types for Underwater Applications.

Antenna Type	Strength	Weakness
Patch Antenna	Compact size; compatible with printed circuit designs; ease of integration; relatively low cost; wide-band response; high gain.	Low radiation efficiency in seawater due to high permittivity and conductivity; Higher frequency of operation introducing stronger attenuation; limited to far-field.
Dipole Antenna	Simple construction; omnidirectional radiation pattern; well-understood behavior in air.	Large size and poor integration capability; poor efficiency in conductive water; limited range; narrow-band response.
MI Loop Antenna	Efficient near-field coupling; immune to multipath and Doppler effects; stable and predictable channel characteristics; lower losses due to magnetic field.	Limited to short-range applications; rapid signal decay with distance; sensitive to alignment due to near-field coupling; huge structure.
Directive Antenna	Focused energy enables better energy saving; higher gain; reduced interference; stealth operation.	Requires alignment; bulky structures; not ideal for dynamic underwater environments.
Magnetoelectric Antenna	Potential for miniaturization; operates efficiently at low frequencies; suitable for stealth and confined spaces.	Still experimental; fabrication complexity; possibility of interference due to acoustical waves; limited practical deployment data; lower power handling.

2.8.2. On Re-Visiting Dipole Waves

The severe attenuation characteristics of seawater remain the dominant limiting factor for long-range underwater communication, constraining the effective operational envelope of most antenna topologies. Nevertheless, numerous experimental studies suggest the feasibility of extended-range communication by exploiting surface waves (Lateral Waves) propagating along the sea-air or sea-seabed interface [21], or through dipole wave mechanisms [15,18]. The central challenge lies in devising novel antenna elements capable of effectively exciting these modes while minimizing near-field dissipation. It has been observed that a significant portion of signal loss (on the order of 60 to 80 dB) occurs within the non-radiating near-field—a sphere extending a few wavelengths from the source—where strong electromagnetic induction generates substantial eddy currents in the conductive medium. However, experiments conducted in [15–18] demonstrate unexpectedly low attenuation rates beyond this near-field region, effectively bypassing the exponential decay expected in bulk seawater. A summary of the measurement results from [15–18] is presented in Figure 14. These findings imply that the losses are driven by field inhomogeneity and near-field ohmic dissipation. Therefore, antenna designs must be optimized to minimize near-field reactive power storage and match closely to far-field plane waves to maximize propagation efficiency.

2.8.3. On Future Challenges

While the optimization of isolated antenna elements is essential, the transition from laboratory prototypes to deployment in realistic marine environments introduces an additional layer of challenges that remains largely underexplored. A critical research gap concerns the scalability of antenna systems for mobile AUV swarms. As underwater networks evolve from point-to-point links to dense, multi-agent swarms, the inherently limited bandwidth of low-frequency antennas—particularly high-Q resonant structures such as magnetic induction coils or magnetoelectric sensors—emerges as a fundamental bottleneck. This narrow operational bandwidth constrains achievable data rates and spectral efficiency, thereby complicating interference mitigation and medium-access control (MAC)

protocols when multiple vehicles attempt simultaneous communication. Consequently, future antenna architectures must explore frequency-agile or reconfigurable designs that enable dynamic spectrum utilization, thereby supporting the scalability and robustness required for large-scale swarm deployments. It is important to note that such systems will typically involve very closely spaced nodes.

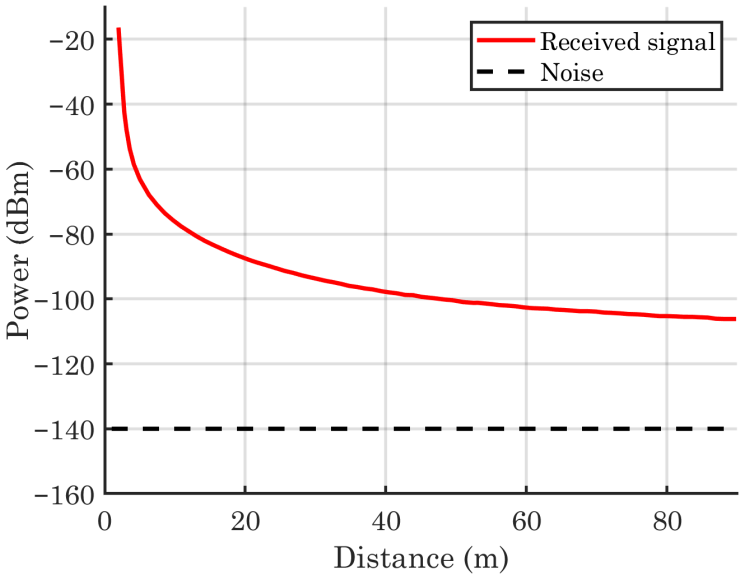

Figure 14. Behavior of a EM signal in seawater for a distance of 100 m at $T = 25$ °C based on the measurements conducted in [17].

The practical deployment constraints of real marine environments pose severe threats to long-term antenna performance, which are often overlooked in simulation-based studies. Beyond well-known attenuation mechanisms, underwater antennas are subject to biofouling, which alters local dielectric boundary conditions and can cause significant impedance detuning—a critical issue for narrowband resonant antennas. Additionally, extreme hydrostatic pressure at depth can mechanically compress antenna substrates, modifying their effective permittivity and shifting the resonant frequency. Future research must therefore focus on pressure-neutral materials, encapsulation strategies, and active compensation circuits capable of dynamically tuning antenna parameters to counteract environmental detuning and corrosion, thereby ensuring consistent performance during extended missions in harsh oceanic conditions.

Furthermore, the realization of effective underwater communication and sensing networks necessitates a holistic system-level design that integrates multiple complementary technologies—namely RF, optical, and acoustic modalities—to compensate for the inherent limitations of each. In this context, RF systems are not intended to replace optical or acoustic links but rather to operate synergistically as complementary channels, providing enhanced quality of service when other modalities degrade or fail. For example, while optical systems can support very high data rates (on the order of Gbps) over short distances in clear water, they experience catastrophic link degradation in turbid environments where RF waves remain comparatively robust. Conversely, acoustic systems enable long-range underwater propagation with relatively low attenuation but suffer from limited data rates and severe multipath effects, particularly near the seabed in cluttered environments. In such scenarios, RF-based communication and sensing systems can be activated to provide higher data rates and more resilient links. Moreover, in sensitive military and security applications, RF communication offers inherent advantages due to the strong attenuation of electromagnetic waves in seawater, which significantly reduces the risk of

interception by adversaries. Despite these advantages, a substantial research gap remains in the development of compact hybrid "triple-mode" systems that seamlessly integrate RF or magnetic radiators with optical and acoustic transceivers. A key challenge for antenna designers lies in exploiting the severely constrained volume of an AUV to maximize RF radiation efficiency without compromising hydrodynamic performance or the functionality of co-located subsystems, thereby enabling robust fallback mechanisms that balance the high throughput of optical links and the long-range capability of acoustic channels with the reliability and security of electromagnetic communication.

3. Conclusions

In this comprehensive review, we evaluated the performance and integration potential of various antenna topologies for underwater communication, ranging from conventional electric dipoles to emerging magnetoelectric (ME) resonators. Our analysis synthesizes the trade-offs between physical size, radiation efficiency, and hydrodynamic compliance required for AUV applications. The primary findings indicate that for low-frequency, size-constrained telemetry ($<$1 MHz), ME antennas are superior to traditional loop antennas, offering gains higher by $>$15 dB and benefiting from constructive image currents when mounted near conductive hulls. Conversely, for high-bandwidth short-range data links ($>$100 MHz), conformal patch antennas are identified as the optimal solution due to their minimal hydrodynamic drag.

However, significant technological gaps persist. Specifically, the practical deployment of ME antennas is currently limited by fabrication complexities—such as interface fragility in composite materials—and a lack of robust array architectures for underwater environments. Furthermore, a complete physical model explaining the low attenuation of lateral surface waves at extended ranges remains to be fully established. Future research directions should focus on two key areas: (1) developing mechanically robust ME arrays to enhance gain through dipole aggregation, and (2) designing novel excitation elements to efficiently couple energy into lateral and dipole wave modes. Finally, for AUV designers, we provide the following practical recommendations: prioritize magnetic-based antennas for low-frequency operations to leverage hull-induced gain enhancement; employ dielectric buffer layers or distilled water encapsulation to isolate the reactive near-field from lossy seawater; and utilize conformal designs to maintain vehicle hydrodynamics. Addressing these challenges will be pivotal in extending the range and reliability of next-generation underwater electromagnetic networks.

Author Contributions: Conceptualization, G.A.K. and D.G.A.; methodology, D.G.A.; validation T.M.E.; formal analysis, D.G.A. and T.N.F.K.; investigation, D.G.A., T.M.E. and D.-N.P.; resources, D.G.A. and D.-N.P.; data curation, Y.K.; writing—original draft preparation, D.G.A. and T.M.E.; writing—review and editing, D.G.A., G.A.K., T.N.F.K. and A.P.; visualization, D.G.A. and T.M.E.; supervision, G.A.K. All authors have read and agreed to the published version of the manuscript.

Funding: This research received no external funding.

Data Availability Statement: Data is contained within the article.

Conflicts of Interest: Authors Dimitrios G. Arnaoutoglou, Yiannis Kyriacou and Andreas Papanastasiou were employed by the company Ecliptic Defence and Space Ltd. The remaining authors declare that the research was conducted in the absence of any commercial or financial relationships that could be construed as a potential conflict of interest.

References

1. Ahmed, A.A.; Najim, A.H.; Al-Dulaimi, A.M.; Ali Alheeti, K.M.; Mohd Satar, N.S.; Aliesawi, S.A. A Review of Key Elements for Underwater Wireless Sensor Networks. In Proceedings of the 2024 International Conference on Decision Aid Sciences and Applications (DASA), Manama, Bahrain, 11–12 December 2024; pp. 1–6. [CrossRef]
2. Hyder, W.; Pabani, J.K.; Luque-Nieto, M.Á.; Laghari, A.A.; Otero, P. Self-Organized Ad Hoc Mobile (SOAM) Underwater Sensor Networks. *IEEE Sens. J.* **2023**, *23*, 1635–1644. [CrossRef]
3. Al Guqhaiman, A.; Akanbi, O.; Aljaedi, A.; Chow, C.E. A Survey on MAC Protocol Approaches for Underwater Wireless Sensor Networks. *IEEE Sens. J.* **2021**, *21*, 3916–3932. [CrossRef]
4. Chen, X.; Tang, J.; Lao, S. Review of Unmanned Aerial Vehicle Swarm Communication Architectures and Routing Protocols. *Appl. Sci.* **2020**, *10*, 3661. [CrossRef]
5. Theocharidis, T.; Kavallieratou, E. Underwater communication technologies: A review. *Telecommun. Syst.* **2025**, *88*, 54. [CrossRef]
6. Ellis, L. How Does Noise Pollution Harm Marine Species. Earth.Org—Global Commons. 2024. Available online: https://earth.org/noise-pollution-in-the-ocean/ (accessed on 5 August 2025).
7. Wang, X.; Zhang, M.; Zhou, H.; Ren, X. Performance Analysis and Design Considerations of the Shallow Underwater Optical Wireless Communication System with Solar Noises Utilizing a Photon Tracing-Based Simulation Platform. *Electronics* **2021**, *10*, 632. [CrossRef]
8. Schirripa Spagnolo, G.; Cozzella, L.; Leccese, F. Underwater Optical Wireless Communications: Overview. *Sensors* **2020**, *20*, 2261. [CrossRef] [PubMed]
9. Rhodes, M. Underwater Electromagnetic Propagation: Re-evaluating Wireless Capabilities. *Hydro Int.* **2006**, *10*, 28–31.
10. Alahmad, R.; Alraie, H.; Hasaba, R.; Eguchi, K.; Matsushima, T.; Fukumoto, Y.; Ishii, K. Performance Analysis of Underwater Radiofrequency Communication in Seawater: An Experimental Study. *J. Mar. Sci. Eng.* **2024**, *12*, 2104. [CrossRef]
11. Hott, M.; Hoeher, P.A.; Reinecke, S.F. Magnetic Communication Using High-Sensitivity Magnetic Field Detectors. *Sensors* **2019**, *19*, 3415. [CrossRef] [PubMed]
12. Naylor, B.; Read, M.; Timmis, J.; Tyrrell, A. The Relay Chain: A Scalable Dynamic Communication Link between an Exploratory Underwater Shoal and a Surface Vehicle. In Proceedings of the 14th International Conference on the Synthesis and Simulation of Living Systems (ALIFE 2014), New York, NY, USA, 31 July 2014; MIT Press: Cambridge, MA, USA, 2014; pp. 290–297. [CrossRef]
13. Orfanidis, S.J. *Electromagnetic Waves and Antennas*; Rutgers University: New Brunswick, NJ, USA, 2004.
14. Che, X.; Wells, I.; Dickers, G.; Kear, P.; Gong, X. Re-Evaluation of RF Electromagnetic Communication in Underwater Sensor Networks. *IEEE Commun. Mag.* **2010**, *48*, 143–151. [CrossRef]
15. Yip, C.; Goudevenos, A.; Lucas, J. Antenna design for the propagation of EM waves in seawater. *Underw. Technol. Int. J. Soc. Underw.* **2008**, *28*, 11–20. [CrossRef]
16. Al-Shamma'a, A.; Shaw, A.; Saman, S. Propagation of electromagnetic waves at MHz frequencies through seawater. *IEEE Trans. Antennas Propag.* **2004**, *52*, 2843–2849. [CrossRef]
17. Shaw, A.; Al-Shamma'a, A.; Wylie, S.; Toal, D. Experimental Investigations of Electromagnetic Wave Propagation in Seawater. In Proceedings of the 2006 European Microwave Conference, Manchester, UK, 10–15 September 2006; pp. 572–575. [CrossRef]
18. Lucas, J.; Yip, C. A determination of the propagation of electromagnetic waves through seawater. *Underw. Technol. Int. J. Soc. Underw.* **2007**, *27*, 1–9. [CrossRef]
19. Kondratiev, I.G.; Kudrin, A.V.; Zaboronkova, T.M. *Electrodynamics of Density Ducts in Magnetized Plasmas: The Mathematical Theory of Excitation and Propagation of Electromagnetic Waves in Plasma Waveguides*, 1st ed.; CRC Press (Taylor & Francis): Boca Raton, FL, USA, 1999; p. 288.
20. Budden, K.G.; Martin, H.G. The ionosphere as a whispering gallery. *Proc. R. Soc. Lond. Ser. A Math. Phys. Sci.* **1962**, *265*, 554–569. [CrossRef]
21. Bush, B.F.; Tripp, V.K.; Naishadham, K. Practical modeling of radio wave propagation in shallow seawater. In Proceedings of the 2012 IEEE International Symposium on Antennas and Propagation, Chicago, IL, USA, 8–14 July 2012; pp. 1–2. [CrossRef]
22. Bui, V.P.; Yeoh, W.S. Propagation and channel characteristics in seawater environment. In Proceedings of the 2014 IEEE Antennas and Propagation Society International Symposium (APSURSI), Memphis, TN, USA, 6–11 July 2014; pp. 701–702. [CrossRef]
23. Kawamura, T.; Matsushita, T.; Kaneko, Y.; Kawai, N.; Matsui, Y.; Horii, A.; Yoshida, H. Conceptual Design and Propagation Characteristics of an Underwater Electromagnetic Communication System for Ocean Environment Sensor Systems. In Proceedings of the 2024 18th European Conference on Antennas and Propagation (EuCAP), Glasgow, UK, 18–22 March 2024; pp. 1–5. [CrossRef]
24. Ren, Y.; Wang, H.; Yang, K. Modeling of Medium- and Long-Range Electromagnetic Communication Channel for Underwater Wireless Sensor Networks. *IEEE Sens. J.* **2024**, *24*, 24865–24879. [CrossRef]

25. Ren, Y.; Wang, H.; Yang, K. Efficient Method for Solving Underwater Electromagnetic Fields Generated by Radiation Sources in Seawater. *IEEE Antennas Wirel. Propag. Lett.* **2024**, *23*, 1638–1642. [CrossRef]
26. Tahir, M.; Yan, P.; Shuo, L. Channel characterization of EM waves propagation at MHz frequency through seawater. *Int. J. Commun. Syst.* **2018**, *31*, e3462. [CrossRef]
27. International Telecommunication Union. *Radio Regulations, Articles, Edition of 2020*; ITU: Geneva, Switzerland, 2020.
28. Fattah, S.; Gani, A.; Ahmedy, I.; Idris, M.Y.I.; Targio Hashem, I.A. A Survey on Underwater Wireless Sensor Networks: Requirements, Taxonomy, Recent Advances, and Open Research Challenges. *Sensors* **2020**, *20*, 5393. [CrossRef] [PubMed]
29. Mohsan, S.A.H.; Li, Y.; Sadiq, M.; Liang, J.; Khan, M.A. Recent Advances, Future Trends, Applications and Challenges of Internet of Underwater Things (IoUT): A Comprehensive Review. *J. Mar. Sci. Eng.* **2023**, *11*, 124. [CrossRef]
30. Patel, S. A Comprehensive Review of Unmanned Underwater Vehicles: Technologies, Applications, and Challenges. *J. Sci. Innov. Adv. Res.* **2025**, *1*, 236–243.
31. Akyildiz, I.F.; Wang, P.; Sun, Z. Realizing underwater communication through magnetic induction. *IEEE Commun. Mag.* **2015**, *53*, 42–48. [CrossRef]
32. Ylinen, J.; Koskela, M.; Iso-Anttila, L.; Loula, P. Near Field Communication Network Services. In Proceedings of the 2009 Third International Conference on Digital Society, Cancun, Mexico, 1–7 February 2009; pp. 89–93. [CrossRef]
33. Shibuya, H.; Tsukuda, T.; Suzuki, H.; Shimizu, T.; Dobashi, M.; Nishizono, S.; Baba, M.; Sasaki, H.; Terajima, K. A wireless charging and near-field communication combination module for mobile applications. In Proceedings of the 2014 IEEE 64th Electronic Components and Technology Conference (ECTC), Orlando, FL, USA, 27–30 May 2014; pp. 763–768. [CrossRef]
34. Lekka, E.A.; Paschaloudis, K.D.; Kyriacou, G.A. Phased array design for near field focused hyperthermia based on reciprocity theorem. In Proceedings of the 2017 International Workshop on Antenna Technology: Small Antennas, Innovative Structures, and Applications (iWAT), Athens, Greece, 1–3 March 2017; pp. 277–280. [CrossRef]
35. Karkanis, N.; Kaifas, T.N.F.; Samaras, T.; Kyriacou, G.A. Comparative Study of Minimally Invasive Microwave Ablation Applicators. *Appl. Sci.* **2025**, *15*, 2142. [CrossRef]
36. Haraldsen, O.R. *Next Generation HUGIN SUPERIOR AUV Raises the Bar for Subsea Survey Data Quality*; Kongsberg Maritime Newsroom: Kongsberg, Norway, 2018.
37. HII. REMUS UUVs (Unmanned Underwater Vehicles). HII Website. 2025. Overview of REMUS UUV Platform, Technical Features, and Applications. Available online: https://www.thalesgroup.com/en/solutions-catalogue/defence/naval/high-performance-scalable-mine-countermeasures?utm_medium=website&utm_source=Google_ads&utm_campaign=Mine%20Countermeasures&utm_content=English%20Webpage&gad_source=1&gad_campaignid=23219788455&gbraid=0AAAAA-2a23PGdqGkOAC_67zBaCwfzM0mV&gclid=Cj0KCQiA9t3KBhCQARIsAJOcR7wYX_Bl74tEJjskK1lLBw3LpddePpQ8T_Ebi5_2iVymKNQmMyqcUoQaAn88EALw_wcB (accessed on 5 December 2025).
38. Teledyne Webb Research. Teledyne Webb Research Oceanographic Instruments. Teledyne Marine Website. 2025. Description of Webb Research Gliders and Oceanographic Instrumentation. Available online: https://www.teledynemarine.com/webb-research (accessed on 5 December 2025).
39. Free3D. Saab Seaeye Sabertooth 3D Model. Free3D Website. 2022. 3D Model of Saab Seaeye Sabertooth Retrieved from Free3D. Available online: https://free3d.com/3d-model/saab-seaeye-sabertooth-5185.html (accessed on 5 December 2025).
40. Balanis, C.A. *Antenna Theory: Analysis and Design*, 4th ed.; John Wiley & Sons: Hoboken, NJ, USA, 2016; p. 1104.
41. Gaoding, N.; Bousquet, J.F. A Compact Magneto-Inductive Coil Antenna Design for Underwater Communications. In Proceedings of the 12th International Conference on Underwater Networks & Systems (WUWNet '17), Halifax, NS, Canada, 6–8 November 2017. [CrossRef]
42. Haga, N.; Chakarothai, J.; Konno, K. Circuit Modeling of Near-Field Coupled Undersea Antennas Using Impedance Double Expansion Method. *IEEE Trans. Antennas Propag.* **2024**, *72*, 9378–9391. [CrossRef]
43. Yang, L.; Ju, M.; Zhang, B. Bidirectional Undersea Capacitive Wireless Power Transfer System. *IEEE Access* **2019**, *7*, 121046–121054. [CrossRef]
44. Li, C.; Ren, X.; Liu, X.; Wu, S.; Qi, M.; Yu, J.; Cai, C. Modeling and Implementation of a Long-Distance Seawater Single-Wire CPT System for Underwater Sensor. *IEEE Trans. Power Electron.* **2025**, *40*, 7603–7614. [CrossRef]
45. Zhou, S.; Pan, G. On Small Dipole Antennas in Lossy Half Space and Undersea Propagation. In Proceedings of the 2024 IEEE Texas Symposium on Wireless and Microwave Circuits and Systems (WMCS), Piscataway, NJ, USA, 3–4 April 2024; pp. 1–4. [CrossRef]
46. Rangraz, P.; Dowling, H.; Bousquet, J.F. A Receiver Array to Reduce the Effects of Misalignment in Magneto-Inductive Communication. In Proceedings of the OCEANS 2024, Halifax, NS, Canada, 23–26 September 2024; pp. 1–6. [CrossRef]
47. Deschamps de Paillette, T.; Gaugue, A. High Data Rate Wireless Underwater Sensors for Environemental Monitoring. In Proceedings of the OCEANS 2019, Marseille, France, 17–20 June 2019; pp. 1–10. [CrossRef]

48. Manteghi, M. An electrically small antenna for underwater applications. In Proceedings of the 2016 IEEE International Symposium on Antennas and Propagation (APSURSI), Fajardo, Puerto Rico, 26 June–1 July 2016; pp. 1745–1746. [CrossRef]
49. Massaccesi, A.; Pirinoli, P. Analysis of antennas for underwater applications. In Proceedings of the 2017 11th European Conference on Antennas and Propagation (EUCAP), Paris, France, 19–24 March 2017; pp. 1907–1910. [CrossRef]
50. Farmer, J.; Moorhead, R.; Tang, B.; Green, R.; Moorhead, J. Underwater Wireless Electromagnetic/Radio Communication using Software Defined Radios. In Proceedings of the OCEANS 2022, Hampton Roads, VA, USA, 17–20 October 2022; pp. 1–7. [CrossRef]
51. King, R.; Iizuka, K. The complete electromagnetic field of a half-wave dipole in a dissipative medium. *IEEE Trans. Antennas Propag.* **1963**, *11*, 275–285. [CrossRef]
52. Hong, Z.; Wang, M.; Zhang, S.; Wang, X.; Liu, B. Study on LF Insulated Dipole Antenna in Seawater. In Proceedings of the 2024 14th International Symposium on Antennas, Propagation and EM Theory (ISAPE), Hefei, China, 23–26 October 2024; pp. 1–3. [CrossRef]
53. Kawamura, T.; Matsushita, T.; Kaneko, Y.; Kawai, N.; Matsui, Y.; Hongo, K.; Ohkur, K.; Horii, A.; Yoshida, H. A High-Efficiency Underwater Dipole Antenna with Spherical Electrodes. In Proceedings of the 2023 IEEE International Symposium on Antennas and Propagation and USNC-URSI Radio Science Meeting (USNC-URSI), Portland, OR, USA, 23–28 July 2023; pp. 1059–1060. [CrossRef]
54. Sato, H.; Fujii, N.; Chen, Q.; Ishii, N.; Takahashi, M.; Suga, R.; Uesaka, K.; Yoshida, H. Dipole antenna with sheath-cover for seawater use. In Proceedings of the 2017 International Symposium on Antennas and Propagation (ISAP), Phuket, Thailand, 30 October–2 November 2017; pp. 1–2. [CrossRef]
55. Kawamura, T.; Matsushita, T.; Kondo, T.; Takeuchi, F.; Hongo, K.; Matsui, Y.; Takinami, T.; Horii, A.; Ohkuri, K. Formulae for the Impedance and Transmission Factor of an Electrically Small Half-Sheath Dipole Antenna Immersed in Seawater. *IEEE Antennas Wirel. Propag. Lett.* **2022**, *21*, 640–644. [CrossRef]
56. Moore, R.K. Radio communication in the sea. *IEEE Spectr.* **1967**, *4*, 42–51. [CrossRef]
57. Huggins, J.S. Improving the Super J-Pole Antenna. Online Post, 2012. Improvement of Collinear J-Pole ("Super-J") by Replacing the Phasing Stub with a Long Coil to Gain Approximately 0.8 dB. Available online: https://www.hamradio.me/antennas/improving-the-super-j.html (accessed on 5 December 2025).
58. Aboderin, O.; Inacio, S.; Santos, H.M.; Pereira, M.R.; Pessoa, L.M.; Salgado, H.M. Analysis of J-Pole antenna configurations for underwater communications. In Proceedings of the OCEANS 2016 MTS/IEEE Monterey, Monterey, CA, USA, 19–23 September 2016; pp. 1–5. [CrossRef]
59. Aboderin, O.; Pessoa, L.M.; Salgado, H.M. Performance evaluation of antennas for underwater applications. In Proceedings of the 2017 Wireless Days, London, UK, 7–9 July 2017; pp. 194–197. [CrossRef]
60. Hao, Z.; Dawei, G.; Guoping, Z.; Gulliver, T.A. The impact of antenna design and frequency on underwater wireless communications. In Proceedings of the 2011 IEEE Pacific Rim Conference on Communications, Computers and Signal Processing, Victoria, BC, Canada, 23–26 August 2011; pp. 868–872. [CrossRef]
61. Aboderin, O.; Pessoa, L.M.; Salgado, H.M. Wideband dipole antennas with parasitic elements for underwater communications. In Proceedings of the OCEANS 2017, Aberdeen, UK, 9–22 June 2017; pp. 1–6. [CrossRef]
62. Gauns, S.; Lokapure, A.; Fernandes, M.; Colaco, J. Performance Analysis of Antennas for Underwater Applications. In Proceedings of the 2025 IEEE International Students' Conference on Electrical, Electronics and Computer Science (SCEECS), Bhopal, India, 18–19 January 2025; pp. 1–7. [CrossRef]
63. Jaafar, A.N.B.; Ja'Afar, H.; Yamada, Y.; Rahman, N.H.A.; Michishita, N.; Zainudin, N.; Sadeghikia, F.; Abdullah, R. Electromagnetic Analysis of Radio Propagation in Fresh Water and Measurement by Axial Mode Helical Antenna at 433 MHz. *IEEE Open J. Antennas Propag.* **2025**, *6*, 1112–1125. [CrossRef]
64. Yang, Y.; Wang, Z.; Wang, S.; Zhou, Q.; Shen, F.; Jiang, H.; Wu, Z.; Zeng, B.; Guo, Z.; Gong, Y. Designing a Water-Immersed Rectangular Horn Antenna for Generating Underwater OAM Waves. *Electronics* **2019**, *8*, 1224. [CrossRef]
65. Yang, Y.; Liu, G.; Shen, F.; Sun, J.; Guo, K.; Guo, Z.; Zhou, Q.; Jiang, H.; Wu, Z.; Zeng, B.; et al. Generating and Detecting Broad-Band Underwater Multiple OAMs Based on Water-Immersed Array. *IEEE Access* **2020**, *8*, 149586–149594. [CrossRef]
66. Arnaoutoglou, D.G.; Empliouk, T.M.; Kaifas, T.N.F.; Chryssomallis, M.T.; Kyriacou, G. A Review of Multifunctional Antenna Designs for Internet of Things. *Electronics* **2024**, *13*, 3200. [CrossRef]
67. Luo, B.; Velvaluri, P.; Liu, Y.; Sun, N.X. Magnetoelectric BAW and SAW Devices: A Review. *Micromachines* **2024**, *15*, 1471. [CrossRef]
68. Liu, Z.; Song, Y.; Yang, X. Research on air-sea cross-medium communication based on mechanical antenna. *J. Phys. Conf. Ser.* **2025**, *2991*, 012026. [CrossRef]
69. Lü, X.; Chen, X.; Zhang, W.; Gu, L.; Bao, W. Acoustically Actuated Compact Magnetoelectric Antenna for Low-Frequency Underwater Communication. *IEEE Trans. Antennas Propag.* **2023**, *71*, 8493–8503. [CrossRef]

70. Wang, S.Y.; Song, G.M.; Dou, G.Q.; Xin, Y.; Feng, S.M.; Dai, C.P. Mechanism and Key Technology of Low-Frequency Magnetoelectric Antenna: A Systematic Review. In Proceedings of the 2024 3rd International Joint Conference on Information and Communication Engineering (JCICE), Fuzhou, China, 10–12 May 2024; pp. 26–32. [CrossRef]
71. Du, Y.; Xu, Y.; Wu, J.; Qiao, J.; Wang, Z.; Hu, Z.; Jiang, Z.; Liu, M. Very-Low-Frequency Magnetoelectric Antennas for Portable Underwater Communication: Theory and Experiment. *IEEE Trans. Antennas Propag.* **2023**, *71*, 2167–2181. [CrossRef]
72. Nan, T.; Lin, H.; Gao, Y.; Matyushov, A.; Yu, G.; Chen, H.; Sun, N.; Wei, S.; Wang, Z.; Li, M.; et al. Acoustically actuated ultra-compact NEMS magnetoelectric antennas. *Nat. Commun.* **2017**, *8*, 296. [CrossRef]
73. Duman, M.; Mert, O.; Özkan, R.; Ramazan, F.; Yılmaz, Y.; Duman, M.; Knypiński, Ł. Examining the Impacts of Different Characteristics of Water on Coplanar Patch Antenna. In Proceedings of the 2025 7th International Congress on Human-Computer Interaction, Optimization and Robotic Applications (ICHORA), Ankara, Turkey, 23–24 May 2025; pp. 1–5. [CrossRef]
74. Yang, M.; Wu, Q.; Zheng, K.; Zhang, S.; Wei, G. Radiation Field Distribution Above Sea Surface of Underwater Microstrip Antenna Array. *IEEE Antennas Wirel. Propag. Lett.* **2024**, *23*, 858–862. [CrossRef]
75. Zali, H.M.; Pasya, I.; Ali, M.T.; Kobayashi, T. Measurement of wideband microstrip underwater antenna performance with buffer layer structure. In Proceedings of the 2017 IEEE 13th Malaysia International Conference on Communications (MICC), Johor Bahru, Malaysia, 28–30 November 2017; pp. 48–52. [CrossRef]
76. Alvertos, K.N.; Karagianni, E.A.; Vardakis, K.D.; Mpountas, T.K.; Kaklamani, D.I. Bow-tie antenna for underwater Wireless Sensor Networks. In Proceedings of the 2017 International Workshop on Antenna Technology: Small Antennas, Innovative Structures, and Applications (iWAT), Athens, Greece, 1–3 March 2017; pp. 323–326. [CrossRef]
77. Karagianni, E. Electromagnetic Waves under Sea: Bow-Tie Antenna Design for Wi-Fi Underwater Communications. *Prog. Electromagn. Res. M* **2015**, *41*, 189–198. [CrossRef]
78. Amit; Vijay, S. Design and Fabrication of a Patch Antenna for Underwater Communications. *Wirel. Pers. Commun.* **2022**, *126*, 2671–2687. [CrossRef]
79. Jha, S.K.; Suraj, P.; Badhai, R.K. Bow-Tie Shaped Meander Line UWB Antenna for Underwater Communication. In *Advances in Intelligent Systems and Computing*; Springer: Singapore, 2021; Volume 1165, pp. 1077–1086. [CrossRef]
80. Harrington, R.F. Effect of antenna size on gain, bandwidth, and efficiency. *J. Res. Natl. Bur. Stand. Sect. D Radio Propag.* **1960**, *64D*, 1–12. [CrossRef]
81. Hassanien, A.E.; Breen, M.; Li, M.H.; Gong, S. A theoretical study of acoustically driven antennas. *J. Appl. Phys.* **2020**, *127*, 014903. [CrossRef]
82. Cui, Y.; Wang, C.; Song, X.; Wu, M.; Zhang, Q.; Yuan, H.; Yuan, Z. A survey of mechanical antennas applied for low-frequency transmitting. *iScience* **2023**, *26*, 105832. [CrossRef]
83. Ippet-Letembet, L.C.; Xu, R.F.; Jeanty, R.; Yao, Z.; Candler, R.N.; Chen, S.Y. Modeling of Multiferroic Antennas in the Akhiezer Regime: Effects of Acoustic Resonator Excitation and Topology on Radiation. *IEEE Trans. Antennas Propag.* **2024**, *72*, 9058–9071. [CrossRef]
84. Liang, X.; Chen, H.; Hu, Z.; Lin, H.; Huang, H.; Guo, J.; Ju, D.; Liu, M.; Sun, N.X. Experimental Demonstration of Ground Plane Immunity for Magnetoelectric Antennas. In Proceedings of the 2022 IEEE MTT-S International Microwave Workshop Series on Advanced Materials and Processes for RF and THz Applications (IMWS-AMP), Guangzhou, China, 13–15 November 2022; pp. 1–3. [CrossRef]
85. Xu, J.; Leung, C.M.; Zhuang, X.; Li, J.; Bhardwaj, S.; Volakis, J.; Viehland, D. A Low Frequency Mechanical Transmitter Based on Magnetoelectric Heterostructures Operated at Their Resonance Frequency. *Sensors* **2019**, *19*, 853. [CrossRef]
86. Niu, Y.; Ren, H. Transceiving Signals by Mechanical Resonance: A Miniaturized Standalone Low Frequency (LF) Magnetoelectric Mechanical Antenna Pair with Integrated DC Magnetic Bias. *IEEE Sens. J.* **2022**, *22*, 14008–14017. [CrossRef]
87. Xiao, N.; Wang, Y.; Chen, L.; Wang, G.; Wen, Y.; Li, P. Low-Frequency Dual-Driven Magnetoelectric Antennas with Enhanced Transmission Efficiency and Broad Bandwidth. *IEEE Antennas Wirel. Propag. Lett.* **2023**, *22*, 34–38. [CrossRef]
88. Niu, Y.; Ren, H. A miniaturized low frequency (LF) magnetoelectric receiving antenna with an integrated DC magnetic bias. *Appl. Phys. Lett.* **2021**, *118*, 264104. [CrossRef]
89. Rostami, F.R.; Khaleghi, A.; Balasingham, I. Computer Simulation of Magnetoelectric Antenna and Performance Comparison with Micro-Loop. *IEEE Access* **2022**, *10*, 64473–64482. [CrossRef]
90. Li, K.; Zhang, Q.; Chang, Y.; Wang, J.; Liu, H.; Zhang, S.; Gu, Y. Improved Performance of Acoustically Actuated Magnetoelectric Antenna with FeGa/FeGaB Bilayer. *Micromachines* **2024**, *15*, 190. [CrossRef]
91. Luo, B.; Sun, N. Magnetoelectric antennas for RF applications. In *Magnetoelectric Composites: Materials, Structures, and Applications*; Srinivasan, G., Priya, S., Sun, N., Eds.; Elsevier: Amsterdam, The Netherlands, 2025; pp. 427–440. [CrossRef]
92. Musa, A.A.; Bello, A.; Adams, S.M.; Onwualu, A.P.; Anye, V.C.; Bello, K.A.; Obianyo, I.I. Nano-Enhanced Polymer Composite Materials: A Review of Nanocomposite Preparation and Properties. *Polymers* **2025**, *17*, 893. [CrossRef]
93. Guckel, H.; Judy, J.W.; Wooley, B.A.; Modlin, S.A. Surface Micromachined Suspended Structures: Fabrication and Reliability Issues. *IEEE Trans. Electron Devices* **1989**, *36*, 2753–2760. [CrossRef]

94. Lal, R.; Schmid, A.; Lutz, M.; Kuper, W.A. Manufacturing yield and reliability in surface-micromachined microstructures. *J. Microelectromech. Syst.* **1998**, *7*, 117–123. [CrossRef]
95. Lin, H.; Zaeimbashi, M.; Sun, N.; Liang, X.; Chen, H.; Dong, C.; Matyushov, A.; Wang, X.; Guo, Y.; Gao, Y.; et al. NEMS Magnetoelectric Antennas for Biomedical Application. In Proceedings of the 2018 IEEE International Microwave Biomedical Conference (IMBioC), Philadelphia, PA, USA, 14–15 June 2018; pp. 13–15. [CrossRef]